

1                   Reconstructed soil moisture droughts in  
2                   Belgium reveal 2011–2020 was the driest  
3                   decade since 1970

4                   Katoria Lekarkar<sup>1\*</sup>, Oldrich Rakovec<sup>2</sup>, Rohini Kumar<sup>3</sup>, Stefaan Dondeyne<sup>1,4,6</sup>  
5                   and Ann van Griensven<sup>1,5</sup>

6                   <sup>1</sup>Department of Water and Climate, Vrije Universiteit Brussel, Pleinlaan 2, 1050,  
7                   Brussels, Belgium.

8                   <sup>2</sup>Faculty of Environmental Sciences, Czech University of Life Sciences Prague,  
9                   Praha-Suchdol, Czech Republic.

10                  <sup>3</sup>UFZ-Helmholtz Centre for Environmental Research, Permoserstraße 15, 04318,  
11                  Leipzig, Germany.

12                  <sup>4</sup>Gembloux Agro-Bio Tech, University of Liège, Pass. des Déportés 2, 5030,  
13                  Gembloux, Belgium.

14                  <sup>5</sup>Water Science & Engineering Department, IHE Delft Institute for Water Education,  
15                  2611 AX, Delft, The Netherlands.

16                  <sup>6</sup>Department of Soil Science and Land Resources, Universitas Padjadjaran, Jawa Barat  
17                  45363, Bandung, Indonesia.

18                                   \*Corresponding author: [katoria.lesaalon.lekarkar@vub.be](mailto:katoria.lesaalon.lekarkar@vub.be);

19                                   **Abstract**

20                   In recent years, Belgium has experienced a sequence of intense droughts  
21                   with wide-ranging impacts across multiple sectors. Determining whether  
22                   these events are unprecedented or within natural variability requires indica-  
23                   tors that properly diagnose drought. Root-zone soil moisture is a suitable  
24                   indicator because it integrates meteorological forcings with land-surface  
25                   processes. In Belgium, however, operational monitoring relies mainly on  
26                   precipitation-based indices and lacks long-term in situ soil-moisture obser-  
27                   vations, leaving uncertainty about whether these indices capture the per-  
28                   sistence of root-zone drought. To address this gap, we reconstructed daily  
29                   root-zone soil-moisture dynamics over Belgium for 1970–2020 using the  
30                   mesoscale Hydrologic Model (mHM), placing recent droughts in histori-  
31                   cal context and evaluating the adequacy of precipitation-based indicators

32 for representing drought conditions. Our analysis shows that droughts in  
33 2011–2020 were unprecedented in both duration and severity over the  
34 past five decades. Between 2011 and 2020, the country experienced a  
35 cumulative three years (non-consecutive) of drought exposure, represent-  
36 ing 30% of the decade. This more than doubles the cumulative duration  
37 in each decade from 1981–2010 and about 1.5 times that of 1971–1980.  
38 We further find that the Standardized Precipitation–Evapotranspiration Index  
39 (SPEI), currently used operationally as a proxy for agricultural droughts in  
40 Belgium, underestimates the persistence of root-zone droughts because it  
41 does not explicitly account for land-surface memory. Thus, by including soil  
42 moisture monitoring in drought assessment, residual stresses on agriculture  
43 and subsurface water which can persist long after meteorological condi-  
44 tions have normalized, can still be detected. This gives decision-makers a  
45 more realistic understanding of droughts and how to respond proportionately.

46 **Keywords:** Mesoscale, climate variability, drought persistence, cumulative exposure,  
47 agricultural drought monitoring

## 48 1 Introduction

49 Belgium has faced a succession of hugely consequential droughts in recent years. These  
50 droughts suppressed crop yields, increased water scarcity, disrupted navigation on inland  
51 waters and caused economic losses running into millions of Euros (Tröltzsch et al., 2016;  
52 De Ridder et al., 2020).

53 The country has faced at least five major droughts between 2011 and 2023. From January  
54 to April 2011, the country had received less than half of the expected rainfall by that time of the  
55 year (European Commission, Joint Research Centre, 2011). This was followed by successive  
56 multi-year droughts in 2016-2017 and then 2018-2019, which compounded water scarcity with  
57 unprecedented temperatures, including a record temperature of 39.7°C in July 2019 (Bastos  
58 et al., 2020; Chini, 2022). The consequences to different sectors were enormous. In the Flem-  
59 ish region (the northern part of the country), the 2018-2019 drought reduced potato production  
60 by 31%, leading to a 23% surge in prices. Sugar beet production also fell by 13% while cereal  
61 yields experienced a 10% decline. These led to farmers submitting claims of about €150 mil-  
62 lion to the Flemish Disaster Fund to compensate for losses from the drought (De Ridder et al.,  
63 2020). According to De Vlaamse Waterweg nv, the agency in charge of inland water in Flan-  
64 ders, inland navigation suffered economic losses exceeding €300 million due to low water  
65 levels in navigable waterways.

66 The country experienced another drought crisis in 2022, where more than 50% of the coun-  
67 try was affected, more than ten times the long-term average impacted area of 4.6% between  
68 2000 and 2020. The conditions were so dry that the country experienced a record low 5 mm

69 precipitation in July that year, the lowest in 137 years (since 1885). The precipitation deficit  
70 drove groundwater levels to their lowest since at least 2000 (DOV, 2025); in many locations,  
71 levels did not fully recover over the following winter (VMM, 2023). Of all European countries,  
72 Belgium was the second most affected country in terms of the proportion of area impacted  
73 by the drought (European Environment Agency, 2023). According to the Copernicus Climate  
74 Change Service (2022), surface soil moisture in Europe throughout 2022 was the second low-  
75 est in the previous 50 years, sustained by higher-than-average temperatures and a sequence of  
76 heatwaves that started in spring and continued throughout summer. The severity of the 2022  
77 season eventually forced the Flemish government to officially declare the drought a disaster to  
78 provide compensation for widespread crop failures.

79 While the impacts of these recent droughts are well documented, their rarity in a multi-  
80 decadal context is less well understood. To place their magnitude and severity in perspective,  
81 it is therefore essential to reconstruct historical drought occurrence over a sufficiently long  
82 climatological period. This long-term view allows us to assess whether recent events represent  
83 unprecedented extremes or fall within the range of natural climate variability.

84 Belgium has an extensive network of precipitation, river discharge and groundwater  
85 monitoring stations which provide the basis for monitoring hydrological and meteorological  
86 droughts. This data underlies the drought indices found in dedicated platforms for tracking and  
87 communicating the evolution of droughts across the country (e.g. [https://www.meteo.be/en/  
88 weather/forecasts/drought](https://www.meteo.be/en/weather/forecasts/drought), <https://vmm.vlaanderen.be/water/droogte>). Due to the lack of long-  
89 term observations of soil moisture in the country, the extent of agricultural droughts is presently  
90 evaluated with the Standardized Precipitation Evaporation Index (SPEI) (Vicente-Serrano  
91 et al., 2010) which expresses anomalies in the climatic water balance, that is, precipi-  
92 tation minus potential evapotranspiration. The nationwide drought conditions are reported  
93 through <https://www.meteo.be/en/weather/forecasts/drought>. Although useful, precipitation-  
94 and temperature-based drought indices are constrained by their limited ability to fully rep-  
95 resent agricultural drought conditions. Firstly, these indices do not explicitly account for the  
96 vertical distribution of water within the root zone that supports plant growth, nor do they  
97 reflect the complex interactions between soil moisture and vegetation across different stages  
98 of plant development and are thus inadequate to represent extreme water shortage that would  
99 lead to biomass and crop yield reduction (Sheffield et al., 2004; Mishra and Singh, 2010;  
100 Samaniego et al., 2013). While soil moisture may exhibit a direct link to precipitation at  
101 monthly timescales, soil moisture responses can be nonlinear at shorter timescales, particularly  
102 during dry conditions. Soil moisture also has a memory effect that can lag precipitation anoma-  
103 lies by days to months and in turn prolong the persistence and severity of drought (Bonan and

104 Stillwell-Soller, 1998; Nicholson, 2000; Wu et al., 2002; Seneviratne et al., 2006). Accord-  
105 ingly, developing indices based on soil moisture offers a more reliable indicator of agricultural  
106 drought, as soil moisture integrates the effects of antecedent precipitation, plant water uptake  
107 through transpiration, and the increasing persistence of soil wetness with soil depth (Wu et al.,  
108 2002; Sheffield et al., 2004).

109 The goal of this study is therefore to perform a retrospective high-resolution reconstruction  
110 of root-zone soil moisture to perform a first-of-its-kind assessment of soil moisture droughts in  
111 Belgium over the five decades between 1970 and 2020. We aim to characterize major droughts  
112 that have occurred over this period by clustering soil moisture anomalies using thresholds that  
113 capture the spatiotemporal characteristics of identified events and rank them based on their  
114 magnitude, spatial extent and duration, and evaluate how drought patterns in the country have  
115 evolved over the five decades. To evaluate the correspondence between SPEI and soil moisture-  
116 based anomalies to represent agricultural droughts, we compare SPEI at different accumulation  
117 periods to a soil moisture index (SMI) (Samaniego et al., 2018) during selected major drought  
118 events.

## 119 **2 Methodology**

### 120 **2.1 Study domain**

121 Belgium is located in Western Europe covering an area of 30,528 km<sup>2</sup>, varying in topogra-  
122 phy from sea level along the North Sea coast to 700 m in the Ardennes-Eifel massif in the  
123 south eastern parts (Figure 1) (Meersmans et al., 2016; Sousa-Silva et al., 2016). The coun-  
124 try experiences a warm temperate maritime climate (Köppen-Geiger Cfb) strongly modulated  
125 by the warming effect of the North Atlantic Drift (Erpicum et al., 2018; Beck et al., 2023).  
126 Data from the Royal Meteorological Institute of Belgium (RMI) shows that mean annual tem-  
127 perature ranges between 13 and 17 °C, varying spatially with elevation and distance inland.  
128 Winters are generally mild, with December–January lows dipping under 5°C but rarely below  
129 freezing conditions for /periods. Winters are colder in the Ardennes region due to a weaker  
130 maritime influence and higher elevation. Summers are moderately warm with July highs peak-  
131 ing around 18°C although extremes above 30°C have occurred in recent years. The country  
132 receives an annual average precipitation of about 800 mm which varies between 700 mm in  
133 the western low lying regions, up to 1400 mm in the Ardennes where precipitation is enhanced  
134 by orographic effects (Erpicum et al., 2018). Temporally, rainfall is fairly evenly distributed  
135 throughout the year (Figure 1), with seasonal patterns dominated by summer convective storms  
136 and winter frontal systems (Brisson et al., 2011; Goudenhoofdt and Delobbe, 2013; Journée  
137 et al., 2015).

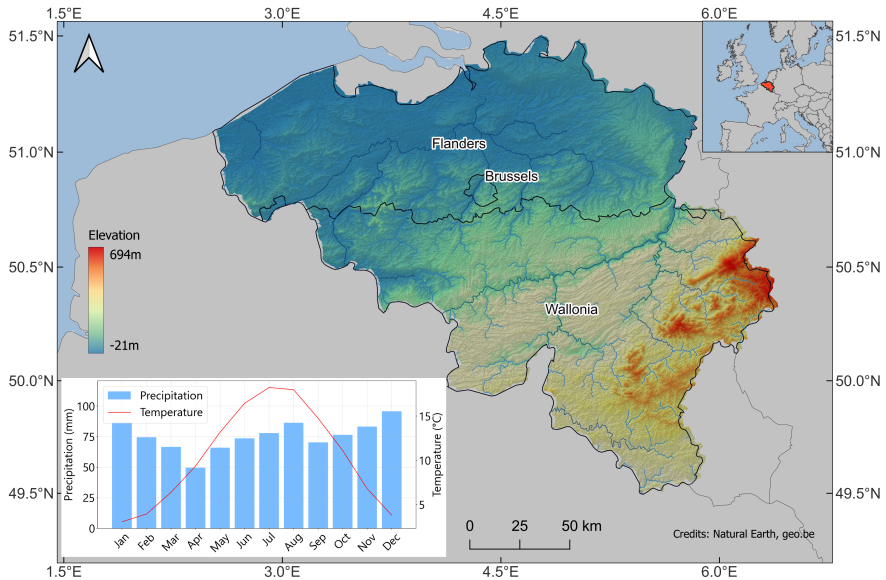


**Fig. 1:** Topographic map of Belgium. The Ardennes region is distinguishable by its high elevation in the south east. Monthly mean precipitation and temperature in the inset plot are derived from data provided by The Royal Meteorological Institute of Belgium for the climatological period 1994-2023.

138 Land cover in the country is predominantly agricultural (44%), dominated by croplands  
 139 and animal husbandry. Cultivated areas dominate the central loamy belt and the northwest of  
 140 the country while the coastal polders typified by heavy soils, are more suited for animal-based  
 141 farming (Beckers et al., 2018, 2020; Statbel, 2025a). Forests cover about 23% of the terri-  
 142 tory (just over 700,000 hectares) with 79.8% in the Walloon region, 19.9% in Flanders and  
 143 0.3% in the Brussels-Capital (Sousa-Silva et al., 2016; Royal Forestry Society of Belgium,  
 144 2025). Most of the lowland forests are dominated by broad-leaved tree species with clusters  
 145 of coniferous forest plantations in the north east. In the Ardennes, forests form a mixed  
 146 broadleaved–coniferous complex in the foothills, gradually transitioning to conifer-dominated  
 147 stands at higher elevations (Royal Forestry Society of Belgium, 2025; Statbel, 2025a). Built-  
 148 up and urbanized areas account for about 20% of the land with most cities dating back to the  
 149 Middle Ages. The average population density of the country is 385 inhabitants/km<sup>2</sup> (Beckers  
 150 et al., 2020; Statbel, 2025b).

## 151 **2.2 The mesoscale Hydrologic Model**

152 In our study, we used the mesoscale Hydrologic Model (mHM; Samaniego et al., 2010; Kumar  
153 et al., 2013) (version v-5.13.2-dev0) to simulate domain-wide root-zone (0-2 m) soil moisture  
154 conditions and streamflow, which we used as an additional hydrologic constraint for validating  
155 basin-scale hydrology at major outlets.

156 mHM is a spatially distributed hydrological model based on numerical representations  
157 of dominant hydrological processes. The model is driven by hourly to daily meteorological  
158 forcings, which include precipitation, air temperature (henceforth simply *temperature*), and  
159 potential evapotranspiration, and accounts for major hydrological processes like snowmelt and  
160 accumulation, canopy storage, evapotranspiration, surface runoff and flood routing, three-layer  
161 soil moisture content, and subsurface storage. To represent spatial variability of inputs and state  
162 variables, the model uses three different spatial resolutions, namely (in order of fine to coarse  
163 resolution) Level-0 ( $L_0$ : small-scale morphology) to represent the main terrain features, geo-  
164 logical features, land cover, and soil properties; Level-1 ( $L_1$ : mesoscale hydrology) to represent  
165 the dominant hydrological processes; and Level-2 ( $L_2$ : large-scale meteorology) to describe  
166 the variability of meteorological forcings. The model harmonizes the data internally using the  
167 multiscale parameter regionalization (MPR; Samaniego et al., 2010). MPR links model param-  
168 eters at  $L_1$  to their corresponding ones at  $L_0$  using non-linear transfer functions that couple  
169 catchment characteristics with global (calibration) parameters to regionalize model hydrologic  
170 parameters at  $L_0$  and link them to their corresponding values at  $L_1$  using upscaling operators  
171 such as arithmetic mean, geometric mean, and harmonic mean (MPR; Livneh et al., 2015).  
172 With this technique, mHM achieves quasi scale-invariant parameters that enable the model to  
173 preserve the spatial variability of state variables and conserve mass balance (Samaniego et al.,  
174 2010, 2011; Kumar et al., 2013; Samaniego et al., 2013). mHM has been successfully used in  
175 multiple studies at scales ranging from river basins (Zink et al., 2017; Dembélé et al., 2020;  
176 Demirel et al., 2024; Banjara et al., 2025), country level (Samaniego et al., 2013; Rakovec  
177 et al., 2019; Boeing et al., 2022) up to continental-scale (Samaniego et al., 2018; Moravec  
178 et al., 2019; Kumar et al., 2025) and global studies (Řehoř et al., 2025; Shrestha et al., 2025).

### 179 **2.2.1 Input data**

180 Our simulation is driven by daily fields of precipitation and temperature from the ENSEM-  
181 BLES gridded dataset (E-OBS) version 30.0e (Cornes et al., 2018), which covers the entire  
182 modelling domain. E-OBS is a daily land-only gridded observational dataset over Europe  
183 which blends station network time series from the European National Meteorological and  
184 Hydrological Services or other sources and is provided with spatial resolutions of  $0.1^0$  and  
185  $0.25^0$ . Our setup uses the  $0.1^0$  resolution product (access url: <https://cds.climate.copernicus.eu/>)

186 datasets/insitu-gridded-observations-europe?tab=download, last accessed March 2025). Since  
 187 E-OBS does not provide potential evapotranspiration data, we generated this from the E-OBS  
 188 minimum and maximum temperature using the method of Hargreaves and Samani (1985).

189 The morphological datasets for the model originate from different sources, namely,  
 190 LAI maps from Global Inventory Modeling and Mapping Studies (GIMMS) (Cao et al.,  
 191 2023), DEM from the Shuttle Radar Topography Mission (Farr et al., 2007), land use data  
 192 from Corine Land Cover (<https://land.copernicus.eu/en/products/corine-land-cover>), soil tex-  
 193 ture and bulk density data from the Harmonized World Soil Database (Nachtergaele et al.,  
 194 2023), and geology datasets from the Global Lithological Map Database (Hartmann and  
 195 Moosdorf, 2012), accessed from the url: [https://www.geo.uni-hamburg.de/geologie/forschung/  
 196 aquatische-geochemie/glim.html](https://www.geo.uni-hamburg.de/geologie/forschung/aquatische-geochemie/glim.html) (last accessed February 2025). To ensure the spatial consis-  
 197 tency required by mHM, we prepared all  $L_0$  datasets at  $0.001953125^\circ$  ( $1/512^\circ$ ), bilinearly  
 198 coarsened the  $L_2$  meteorological data to  $0.125^\circ$  ( $1/8^\circ$ ), and set the resolution of  $L_1$  to  $0.03125^\circ$   
 199 ( $1/32^\circ$ ), these are summarized in Table 1. We then run the model from 1965 to 2020, including  
 200 a warm-up period of 5 years at the beginning.

201 Long-term in situ soil moisture data to validate the soil moisture output of mHM is  
 202 not available within Belgium; so we expanded the model domain to cover parts of France,  
 203 Germany and the Netherlands, where soil moisture observations are available from the Inter-  
 204 national Soil Moisture Network (ISMN) (Dorigo et al., 2021). From the ISMN, we used data  
 205 from the following networks: COSMOS (Zreda et al., 2008), GROW (Xaver et al., 2020),  
 206 TERENO (Bogena et al., 2018), BFG\_Nw and ORACLE, all shown in Figure 2.

**Table 1:** Summary of data sources

Dataset	Resolution (degrees)	Input format	Source
Meteorological data	1/8	NetCDF	E-OBS v30.0e
Leaf Area Index	1/512	NetCDF	GIMMS
DEM	1/512	ASCII Grid	SRTM
Geology	1/512	ASCII Grid	Global Lithological Map Database
Land Cover	1/512	ASCII Grid	Corine Landcover
Soil texture	1/512	ASCII Grid	Harmonized World Soil Database

## 207 **2.2.2 mHM Soil Moisture simulation**

208 mHM calculates water infiltration between soil layers using an exponential function that  
 209 accounts for the nonlinearity of soil water retention (Samani et al., 2010; Livneh et al.,  
 210 2015). Briefly, for a given soil layer,  $k$ , on pervious areas, the infiltration  $I_k$  into the layer is  
 211 determined by the equation:

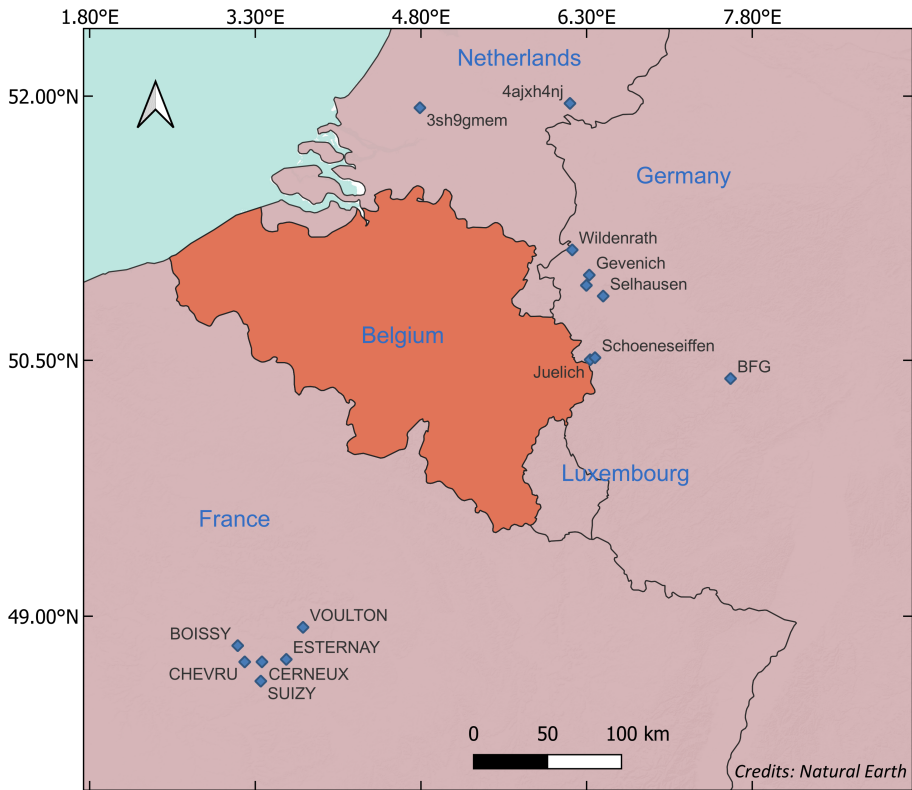


**Fig. 2:** Locations of ISMN stations (blue diamonds) used to validate mHM soil moisture

$$I_k = I_{k-1} * \left( \frac{\theta_k}{\theta_{sat,k}} \right)^{\beta_k} \quad (1)$$

212  $I_{k-1}$  represents the infiltration from the previous layer  $k - 1$ ,  $\theta_k$  is the soil moisture of layer  
 213  $k$ ,  $\theta_{sat,k}$  is the saturation moisture content for the layer, and  $\beta_k$  is an exponential parameter that  
 214 adjusts for the non-linear nature of soil moisture retention. Once infiltration is calculated, the  
 215 model updates soil moisture  $\theta_t$  by adding the difference between the layer infiltration  $I_t$  and  
 216 actual evapotranspiration ( $ET_t$ ) for the time step as;

$$\theta_t = \theta_{t-1} + I_t - ET_t \quad (2)$$

217 Actual evapotranspiration is calculated by reducing the potential evapotranspiration (PET)  
 218 based on a soil moisture stress factor,  $f_{SM}$ , which varies depending on the soil moisture content.

$$ET = f_{roots} \cdot f_{SM} \cdot PET \quad (3)$$

219  $f_{roots}$  is the fraction of roots in the soil horizon and  $f_{SM}$  is calculated using either the Feddes  
 220 equation (Feddes, 1982):

$$f_{SM} = \frac{\theta - \theta_{pwp}}{\theta_{fc} - \theta_{pwp}} \quad (4)$$

221 or the Jarvis equation (after Jarvis (1989)):

$$f_{SM} = \frac{1}{\theta_{stress-index-C1}} \cdot \frac{\theta - \theta_{pwp}}{\theta_{sat} - \theta_{pwp}} \quad (5)$$

222 The model uses the MPR routine to compute the saturation moisture content, field capacity  
 223 ( $\theta_{fc}$ ) and wilting point ( $\theta_{pwp}$ ).

### 224 2.2.3 Model evaluation

225 The accuracy and spatial representativeness of absolute soil moisture values are strongly  
 226 source-dependent (in situ or modelled), so direct comparisons between different datasets can  
 227 be misleading (Koster et al., 2009; Ford and Quiring, 2019). On one hand, simulated soil  
 228 moisture is highly dependent on the quality of meteorological forcings and the physical param-  
 229 eterisation of the model (Koster et al., 2009; Wang et al., 2011a; Nicolai-Shaw et al., 2015). On  
 230 the other hand, in situ measurements are highly localized to the sensor location and are affected  
 231 by the technology used by the sensor and the sufficiency of the calibration techniques (Peng  
 232 et al., 2025). From a drought analysis perspective, the real information value of soil moisture  
 233 is not in its absolute values but rather in its temporal variability metrics, such as anomalies  
 234 and seasonal variability of soil wetness (Koster et al., 2009). This information value is gener-  
 235 ally more consistent and transferable between different sources when soil moisture is suitably  
 236 normalised to have the same range and variability (Dirmeyer et al., 2004; Wang et al., 2011b).  
 237 Koster et al. (2009) show that if soil moisture from different sources differs only in their mean  
 238 and standard deviation, then standardizing each time series (as in Equation 6) would generate  
 239 nearly identical datasets of standard normal deviations ( $\theta'$ ).

$$\theta' = \frac{\theta - \theta_m}{\sigma_m} \quad (6)$$

240 Where  $\theta$  is the soil moisture at a given point and time of year,  $\theta_m$  and  $\sigma_m$  are the mean and  
 241 standard deviation of soil moisture, respectively, for the same point and time of year.

242 In our evaluation of the mHM soil moisture, we used this approach to analyze the level of  
 243 temporal agreement between the standard normal deviations of mHM and in situ soil moisture  
 244 from the corresponding depths at the selected ISMN stations (Figure 2).

245 For each in situ–modelled pair, we quantified the agreement in drought anomaly dynamics  
 246 by calculating the Pearson correlation coefficient ( $r$ ). To obtain an overall agreement across all

247 sites, we first transformed the  $r$  values to the Fisher  $z$ -scale ( $z = \text{arctanh}(r)$ ) to stabilize variance  
248 and avoid bias from the nonlinear  $r$ -scale. The  $z$ -values were then averaged to obtain  $\bar{z}$ , and  
249 finally back-transformed to yield  $\bar{r} = \tanh \bar{z}$ .

250 Prior to the comparison, we performed a quality check on the in situ data to flag and  
251 exclude potentially erroneous measurements. We considered only errors due to systematic drift  
252 in measurements over time (jumps or drops) and spiky measurements that are not explained by  
253 random noise. Here we used the quality control algorithms on in situ soil moisture developed  
254 by Dorigo et al. (2013) considering only stations that have at least 10 years of observations.

255 Because soil moisture is also coupled with runoff through the terrestrial water budget,  
256 we added an independent check for model simulations against daily river-discharge obser-  
257 vations from the major river basins in Belgium. For this we used the inbuilt calibration  
258 feature of mHM and calibrated the model using data from river gauging stations all over the  
259 country, obtained from the Waterinfo database for Flanders ([https://waterinfo.vlaanderen.be/](https://waterinfo.vlaanderen.be/Meetreeksen)  
260 [Meetreeksen](https://waterinfo.vlaanderen.be/Meetreeksen), last accessed March 2025) and the hydrometric network of discharge in Wallonia  
261 (<https://hydrometrie.wallonie.be/home/observations/debit.html?>, last accessed May 2025). In  
262 total we used 91 gauging stations during the calibration period (2000–2023) and 155 stations  
263 to validate the model from 1970–1999.

## 264 **2.3 Characterizing soil moisture droughts**

265 To characterize soil moisture droughts, we use a monthly soil moisture index (SMI), following  
266 Samaniego et al. (2013), considering the total soil water content of the root zone up to a depth  
267 of 0.5 m (We limit our analysis to this depth since groundwater in some regions is shallower  
268 than 0.5m). For each month, grid cell soil moisture is expressed as a percentile relative to that  
269 month’s historical soil moisture and scaled to a range between 0 and 1.

270 The computation of SMI in this study is based on the methodology of Samaniego et al.  
271 (2010), which proceeds as follows. Firstly, the monthly soil moisture averaged over the root-  
272 zone depth (0.5 m for this study) is extracted and used to compute a probability distribution  
273 function (PDF)  $f_i(x)$  for each grid cell as;

$$f_i(x) = \frac{1}{nh} \sum_{k=1}^n K\left(\frac{x-x_k}{h}\right) \quad (7)$$

274 Where,  $x$  is the soil moisture value at which the PDF is evaluated  $x_1, \dots, x_k$  represent the  
275 simulated monthly soil moisture values for the month  $t$  over the simulation period. Note that  
276 this conversion is done for each calendar month separately to account for inherent seasonality  
277 in SM simulations.  $K$  is a Gaussian kernel function and  $h$  is the bandwidth that controls the  
278 smoothness of the kernel (equation 8). The optimal value of  $h$  is computed using a cross-  
279 validation criterion.

$$K(x, x_k) = \frac{1}{\sqrt{2\pi h^2}} \exp\left(-\frac{(x - x_k)^2}{2h^2}\right) \quad (8)$$

280 The monthly grid cell SMI is then derived by integrating  $f_i(x)$  and the resulting SMI val-  
 281 ues are classified into percentiles. Drought-affected grid cells are identified using a threshold  
 282 percentile  $\tau$ , which is commonly set at 0.2 (e.g., Svoboda et al. (2002); Samaniego et al. (2013,  
 283 2018)). This means that for a given month, a grid cell is experiencing drought if the soil mois-  
 284 ture value falls below the  $20^{th}$  percentile of values for that month. According to Svoboda et al.  
 285 (2002), this percentile represents the threshold at which the magnitude of drought begins to  
 286 damage crops, cause water shortages and present high risks of fire. Next, adjacent cells where  
 287  $SMI \leq \tau$  (henceforth denoted as  $SMI_\tau$ ) at each timestep are consolidated to form drought clus-  
 288 ters, which are defined by a minimum threshold area. Spatial clusters which share a minimum  
 289 overlapping area at consecutive time steps are then joined to form multi-temporal clusters,  
 290 each with a unique identity. For each cluster, the mean duration (months), areal extent from the  
 291 onset to termination, and the total drought magnitude, which is the spatiotemporal integral of  
 292  $SMI_\tau$  over the area affected, are computed. Following Samaniego et al. (2013), the magnitude  
 293 of each event is computed as the space-time integral of the drought duration in months over  
 294 the area under drought. This is represented mathematically as;

$$TDM = \sum_{t=t_0}^{t_1} \int_{A_t} [\tau - SMI_i(t)]_+ \quad (9)$$

295  $t_0$  and  $t_1$  represent the onset and termination month of a multi-temporal drought event,  $A_t$   
 296 is the area under drought at timestep  $t$  expressed as a percent of the total domain area, and '+'  
 297 means the magnitude is computed only for the positive part of the function. To avoid detecting  
 298 small, isolated and short-lived dry spells as droughts, we specified a minimum threshold area  
 299 of 640 square kilometres (about 2% of total domain area) based on Samaniego et al. (2013) for  
 300 an event to be considered as a drought, and an overlap area of the same size for two drought  
 301 events at successive time steps to be considered as a single multi-temporal drought cluster.

## 302 **3 Results**

### 303 **3.1 Model Performance Evaluation**

304 The daily standardized anomalies of mHM-simulated soil moisture evaluated against in situ  
 305 observations from the ISMN are shown in Figure 3. Of the 48 stations where in situ data was  
 306 retrieved, 21 sites passed quality-control checks and were retained for validating the model out-  
 307 puts. The resulting comparison showed that the two datasets are highly temporally correlated,  
 308 with a mean Pearson  $\bar{r}=0.86$  (back-transformed averages from the Fisher z-scale), although  
 309 the strength of the correlation varied with sensor depth and type. The correlation is lowest for

310 the top 50 mm of the soil profile ( $\bar{r}=0.81$  for all networks) and increases to 0.86 for the profile  
311 depths greater than 150 mm.

312 Even for the selected in situ sites, some still exhibited spurious spikes outside of random  
313 noise (shown by the red scatter points in Figure 3). We chose not to discard these points so  
314 as to preserve an adequate number of validation stations and to highlight the practical diffi-  
315 culty of obtaining perfectly reliable reference soil moisture data for validating model outputs.  
316 Despite such outliers, the model simulations and ISMN observation showed similar temporal  
317 variability in soil wetness and dryness. The difference mainly occurred in the top 50 mm layer  
318 during very dry episodes when mHM produced more extreme negative anomalies than most  
319 sensors (Figure 3 (a-d)). This explains why the correlation between the datasets is the lowest at  
320 this depth. We attribute this divergence partly to a flooring effect of capacitive sensors, which  
321 tend to plateau at very low volumetric water contents, whereas the model continues to resolve  
322 further drying. For deeper layers, the intensity and duration of dryness were more consistent  
323 between both datasets.

324 To evaluate how well the model simulates drought conditions, we investigated the drought-  
325 day detection skill (when the observed standardized anomaly fell below its 20th percentile)  
326 by counting hits ( $H$ ; days when both model and observations indicate drought), misses ( $M$ ;  
327 observed drought days not flagged by the model), false alarms ( $F$ ; days flagged as drought by  
328 the model but not by the observations), and correct negatives ( $C$ ; days when both indicate non-  
329 drought). (The methodology is described in more detail in Supplementary Text S1). From this  
330 analysis, we found that the model shows high skill in reproducing observed drought conditions,  
331 as it was able to detect 74% of observed drought days from the 21 stations. The false alarm rate  
332 was also only 5%, while the mean  $F_1$  score (which summarizes the balance between misses and  
333 false alarms as  $2H/(2H + F + M)$ ) was 75%. We attribute the differences in detecting droughts  
334 to the scale mismatch between mHM soil moisture, which represents average conditions over  
335 a grid cell, and the highly localized nature of point in situ measurements. Nevertheless, these  
336 metrics indicate that the model can be applied to study droughts.

337 Regarding streamflow performance, the model shows good and spatially consistent skill  
338 across the entire modelling domain and thus provides a reliable basis for analysing soil mois-  
339 ture dynamics. We evaluated daily discharge at 168 gauging stations. During calibration, the  
340 mean Nash-Sutcliffe Efficiency (NSE) across stations was 0.62, with 80% of stations achiev-  
341 ing  $NSE \geq 0.5$  (a commonly used benchmark for satisfactory streamflow simulation). Model  
342 performance during the validation period was also comparatively good, with a mean NSE of  
343 0.63 and 83% of stations recording  $NSE \geq 0.5$ . The full details of the streamflow evaluation,  
344 including the NSE definition, are provided in Supplementary Text S2 (Figure S1).

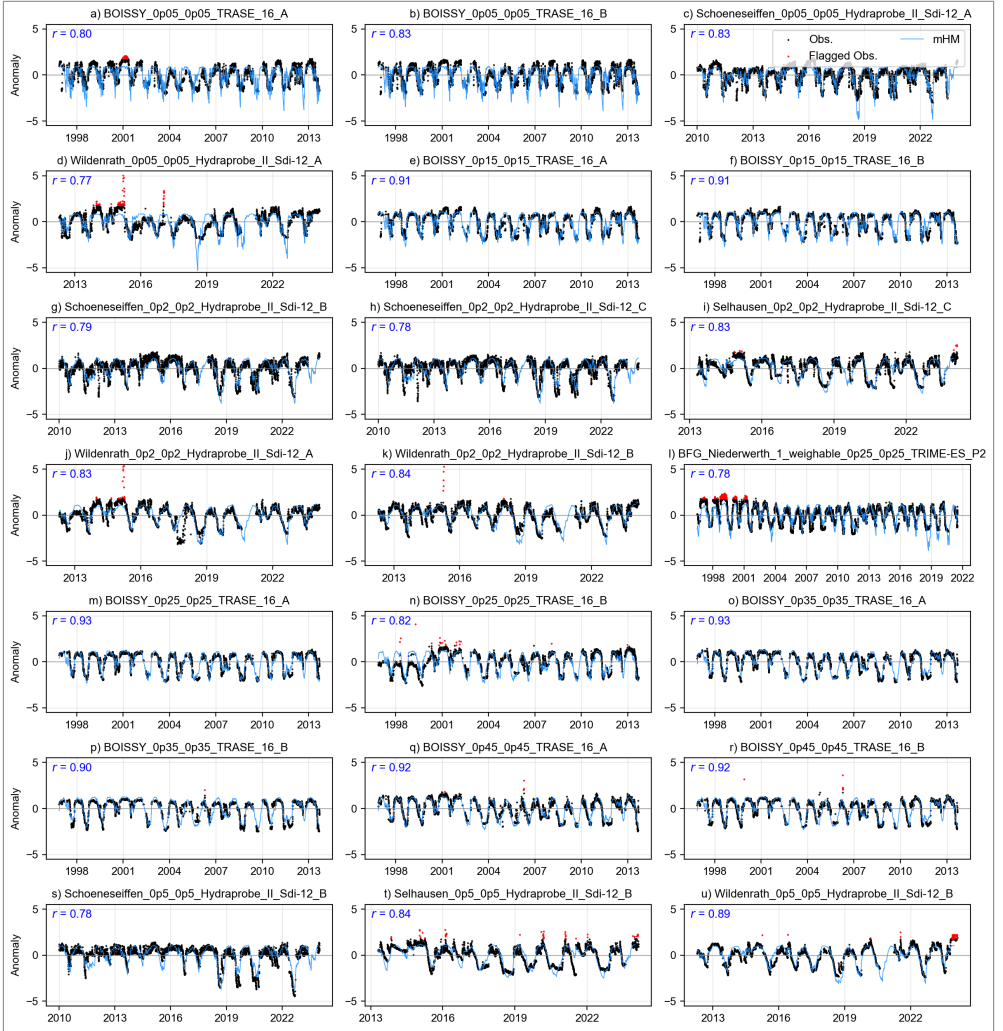


**Fig. 3:** Comparison of standardized anomalies between mHM and in situ soil moisture at selected ISMN sites, ordered by increasing sensor depth. The red scatter points represent observed soil moisture values flagged as potentially erroneous. Titles follow the format `station_topdepth_bottomdepth_sensortype`, e.g., `BOISSY_0p05_0p05_TRASE_16_A` refers to the Boissy station with a sensor at 0.05 m depth and sensor type TRASE.

## 3.2 Decadal evolution of soil-moisture droughts

To summarize how soil-moisture drought behaviour evolves across decades, we use three complementary metrics. First, we quantify the magnitude of each event using the Total Drought Magnitude (TDM), which integrates drought severity over space and time and thus allows drought events to be ranked consistently (Section 3.2.1). Second, in Section 3.2.2, we describe how drought severity is distributed by quantifying the fraction of drought-affected area falling into different severity classes (moderate, severe, extreme, and exceptional) within each decade. These classes capture shifts in the composition of drought conditions beyond just the total magnitude. Third, in Section 3.2.3, we quantify cumulative drought exposure as the total number of months in which each grid cell experiences drought per decade (months need not be consecutive). This metric summarizes how frequently drought conditions recur at a given location over a decade. For decadal summaries, we defined decades starting from 1971 (i.e., 1971–1980) since SPEI construction requires accumulated water-balance anomalies over preceding months (January 1970 will thus not have SPEI-1 values, while January–March 1970 lacks SPEI-3 values. The first year with complete SPEI values is 1971).

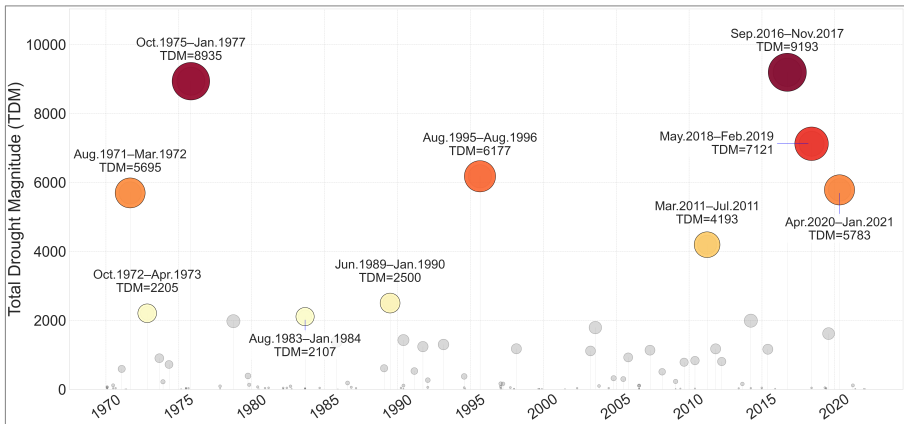
### 3.2.1 Magnitude-based ranking of soil-moisture drought events

Figure 4 shows the magnitude of simulated soil moisture droughts in Belgium between 1970 and 2020 based on the Total Drought Magnitude (TDM), the cumulative deficit in soil moisture below the drought threshold ( $SMI \leq 0.20$ ), integrated over the affected area and the event duration. To ensure an unambiguous severity ranking, the events are ranked by TDM and when two events have similar TDM (difference  $< 1\%$ ), ranks are resolved using a fixed tie-breaker hierarchy: (i) average drought area (fraction of the domain with  $SMI \leq 0.20$  averaged over the entire event), (ii) duration, and (iii) exceptional-class exposure (fraction of  $SMI \leq 0.020$  summed over the duration of the event). On the basis of this ranking, Table 2 displays the corresponding metrics for the ten largest droughts during the period of analysis. From an interdecadal perspective, Figure 4 reveals three distinct drought regimes. Beginning with the 1970s, three major drought events are apparent, dominated by the historic 1975–1977 drought. Although this event is commonly referred to as the 1976 drought, probably because that is when it peaked, the analysis shows that its development in Belgium began back in the autumn of 1975 and lasted for a record 16 months until the winter of 1977. By the end of the event, almost 63% of the domain had experienced drought conditions, although this fluctuated over time<sup>1</sup>. This event established a benchmark against which subsequent droughts in many parts

---

<sup>1</sup>The 63% figure is the mean fraction of the domain affected across all time steps during the drought; at individual times coverage ranged below and above this value, with a maximum of complete (100%) coverage when the drought peaked

377 of Europe are commonly compared. Our analysis reflects this, as this event almost matches the  
378 most intense drought in Belgium during the period of our analysis.



**Fig. 4:** Duration and magnitude of drought events from 1970 to 2020. Each circle represents a drought event, positioned according to its start date (x-axis). The circle size is proportional to the Total Drought Magnitude (TDM) of each event. The ten most severe droughts, ranked by TDM, are highlighted with coloured markers, with their corresponding periods annotated. Events are ranked primarily by TDM; when two events have similar TDM (difference  $\leq 1\%$ ), ranks are determined by peak affected area, then duration, then exceptional-class exposure (defined as  $SMI \leq 0.02$ ).

379 The subsequent three decades (1981–1990, 1991–2000, and 2001–2010) are characterized  
380 by a comparatively wetter hydroclimatic regime, reflected in the lower-magnitude drought  
381 events in Figure 4. Only three events from this period appear in the top ten, and all rank  
382 relatively low by TDM. The largest of these, the 1995–1996 drought, nonetheless persisted for  
383 13 months.

384 A significant shift in drought frequency and severity emerged after 2011. Of the ten biggest  
385 droughts from 1971, four of them were recorded between 2011 and 2020, three of which  
386 occurred in rapid succession between 2016 and 2020. The 2016–2017 drought is the biggest  
387 in this period, exceeding even the 1975–1977 drought by TDM and affected area (64%) and  
388 lasting nearly as long (15 months), as shown in Table 2. The 2018–2019 drought also ranks  
389 among the most severe events, exceeded in TDM only by the 2016–2017 and 1975–1977  
390 droughts (Table 2). Although it persisted for only 10 months, it affected a large fraction of

**Table 2:** The ten biggest soil moisture drought events in Belgium ranked by Total Drought Magnitude.

Rank	Event period	TDM	Average affected area (%)	Duration (months)	Exceptional class exposure (%-mo)
1	Sep 2016–Nov 2017	9193.14	64.0	15	182.9
2	Oct 1975–Jan 1977	8934.97	62.6	16	103.4
3	May 2018–Feb 2019	7120.88	73.1	10	108.3
4	Aug 1995–Aug 1996	6177.27	60.3	13	69.8
5	Apr 2020–Jan 2021	5782.83	58.0	10	27.7
6	Aug 1971–Mar 1972	5694.68	72.9	8	57.3
7	Mar 2011–Jul 2011	4192.92	81.6	5	84.9
8	Jun 1989–Jan 1990	2500.37	51.5	8	8.0
9	Oct 1972–Apr 1973	2204.63	35.4	7	11.2
10	Aug 1983–Jan 1984	2107.37	47.0	6	22.4

391 the domain on average (73%). Although some big droughts have occurred after 2020, we have  
 392 excluded these from our inter-decadal analysis because the current decade is still incomplete.

### 393 3.2.2 Decadal shifts in drought severity

394 While TDM provides a good event-ranking metric, it aggregates drought conditions over space  
 395 and time and therefore does not directly indicate whether severity arises from widespread  
 396 moderate drought or short periods of extreme conditions. To resolve this, we classified all the  
 397 drought events into four severity classes following Svoboda et al. (2002): moderate drought  
 398 ( $0.1 < \text{SMI} \leq 0.2$ ), severe drought ( $0.05 < \text{SMI} \leq 0.1$ ), extreme drought ( $0.02 < \text{SMI} \leq 0.05$ ),  
 399 and exceptional drought ( $\text{SMI} \leq 0.02$ ). We then examined how the severity of droughts have  
 400 evolved within and across decades, as shown in Figure 5. For conciseness we will examine the  
 401 changes at both ends of the drought severity spectrum.

402 As Figure 5 shows, droughts during 1971–1980 were predominantly moderate ( $0.1 <$   
 403  $\text{SMI} \leq 0.2$ ). When exceptional droughts occurred, they remained spatially limited, peaking at  
 404 below 30% of the domain during the 1971–1972 and 1975–1977 events (shown by the black  
 405 dots in Figure 5). As the figure shows, these two droughts were disrupted by wetter spells  
 406 which allowed re-establishment of normal to wet soil moisture conditions between drought  
 407 phases. When accumulated over the decade, moderate droughts accounted for almost 80%  
 408 of all grid-cell months affected by drought, whereas exceptional drought contributed  $\sim 3\%$ ,  
 409 largely associated with the 1975–1977 event (donut plots in Figure 5).

410 Between 1981 and 2010, the drought regime is characterized by predominantly normal-to-  
 411 wet conditions interspersed with episodic, short-lived droughts. Decadal aggregates indicate  
 412 that at least 80% of drought-affected grid-cell months during this period were moderate in

413 intensity, whereas exceptional drought contributed on average less than 1% (Figure 6). How-  
414 ever, individual events (e.g., the 1995–1996 drought) still exhibited brief peaks of exceptional  
415 drought extent when exceptional conditions reached  $\sim 30\%$  of the domain (Figure 5).

416 By contrast, the 2011–2020 period experienced more frequent and severe droughts, par-  
417 ticularly towards the end of the decade (Figure 5). In comparison to the previous decades,  
418 the spatial footprint of exceptional droughts noticeably increased. At the peak of the 2011  
419 droughts, exceptional droughts affected close to 70% of the domain, while during the 2016–  
420 2017 drought, about 40% of the drought-affected area was under exceptional drought, which  
421 did not previously occur even during the 1975–1977 event. This increase is reflected in the  
422 decadal drought area severity, where exceptional droughts accounted for 5.9% of drought-  
423 affected area, a proportion that exceeds all the previous four decades combined (Figure 5).

424

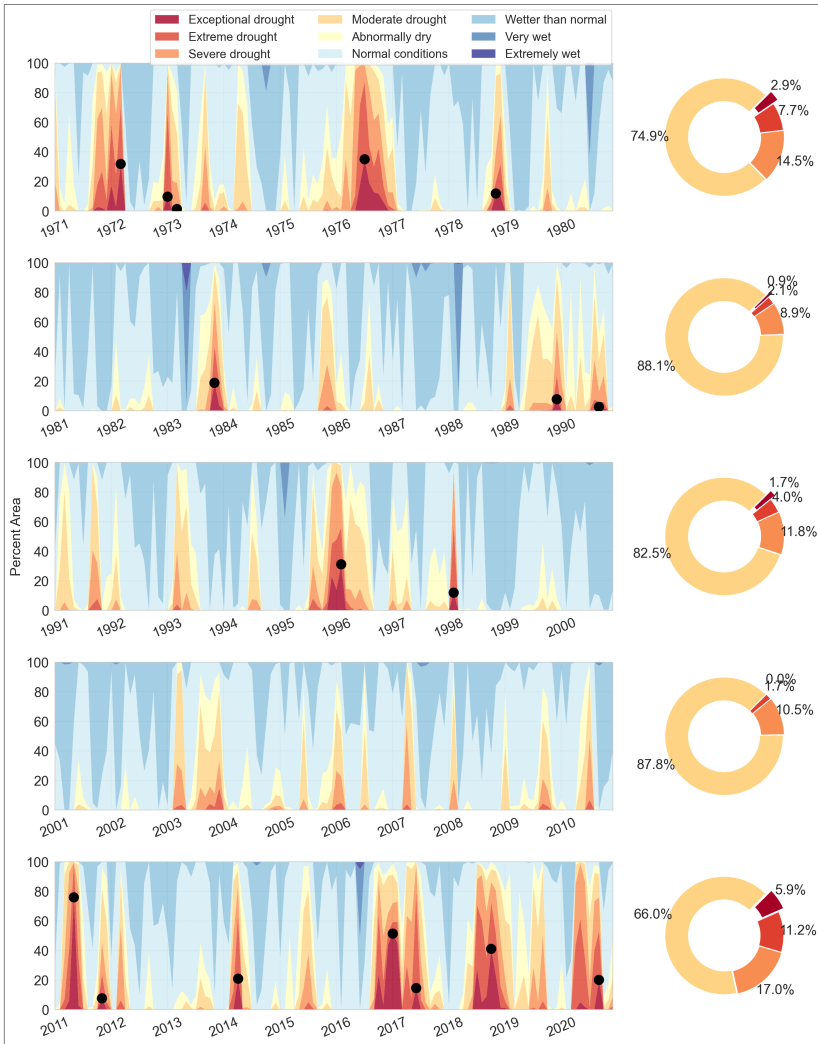


**Fig. 5:** Decadal evolution of drought severity in Belgium, 1971–2020. The stacked panels (left) show the monthly percentage of land area in each soil-moisture class. Black dots mark the peak extent of exceptional drought ( $SMI \leq 0.02$ ). The donut charts (right) summarize, for drought months only ( $SMI \leq 0.20$ ), the mean share of drought-affected area in each drought class; months without drought contribute no area.

### 3.2.3 Decadal drought exposure

Complementing the temporal and spatial analyses, Figure 6 illustrates decadal cumulative drought exposure, expressed as the total number of months in which each grid cell experienced  $\text{SMI} \leq 0.2$  in a decade. The results agree with those of the previous analysis. During 1971–1980, the domain accumulated between 12 and 36 drought months, with a domain-wide mean of about 24 months per grid cell (2.4 months/year) (Figure 6 inset histogram).

Domain-wide improvements in moisture conditions are apparent in the next three decades. The mean cumulative totals fell to 13 months in 1981–1990 (1.3 months/yr), 17 months in 1991–2000 (1.7 months/yr.), and 14 months in 2001–2010 (1.4 months/yr).

As with the other metrics, cumulative drought exposure peaked in 2011–2020. The domain accumulated between 24 and 48 months of drought over the decade, and the domain-wide mean rose to 37 months, or 3.7 months per year (Figure 6). To put this into perspective, this amounts to roughly three continuous years of soil-moisture drought within the decade. This cumulative exposure is more than twice that of each of the three preceding decades (1981–1990, 1991–2000, 2001–2010) and about 1.5 times higher than the previous driest decade, 1971–1980.

To test whether 2011–2020 was statistically drier than the preceding four decades, we applied a non-parametric bootstrap to the per-pixel cumulative drought durations ( $\text{SMI} \leq 0.20$ ) and to the subset of exceptional drought months ( $\text{SMI} \leq 0.02$ ). For each decade, we generated 100,000 bootstrap samples by resampling grid-cell drought durations with replacement, calculated the mean for each sample, and used the 2.5<sup>th</sup> and 97.5<sup>th</sup> percentiles of the resulting distribution to derive the 95% confidence interval (CI) of the sample mean.

The statistical analysis concludes that 2011–2020 was indeed the driest decade of the five decades, both in terms of total drought duration and exposure to exceptional droughts. Over the decade, Belgium accumulated a mean drought period of 37 months (CI: 36.9–37.2 months), significantly higher than in 1971–1980 (mean=25.65 months [CI: 25.6–25.8]), which is the next driest decade (Figure 7 (a)). The lower bound of the 2011–2020 decade CI lies 11 months above the upper bound of the 1971–1980 period and far higher than those experienced in the three decades in between (1981–1990: mean 13 months [CI: 12.92–13.15], 1991–2000: mean 16.9 months [CI: 16.80–16.95] and 2001–2010: mean 13.52 months [CI: 13.46–13.59]).

A similar contrast emerges for the most severe drought (Figure 7(b)). The 2011–2020 decade accumulated 4.3 months of exceptional drought on average (CI: 4.28–4.38), more than the combined total of the four earlier decades. None of the previous decades reached a mean of 2 months of exceptional droughts. 1971–1980 accumulated 1.94 months (CI: 1.89–1.98), 1981–1990 only 0.35 months (CI: 0.34–0.36), 1991–2000 0.80 months (CI: 0.79–0.84), and

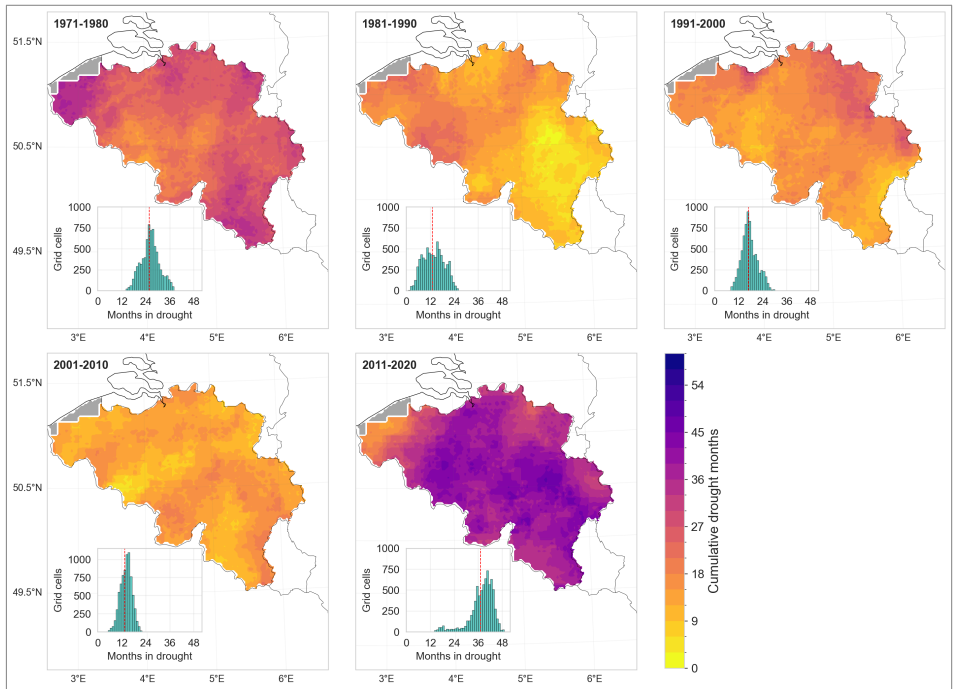


**Fig. 6:** Cumulative decadal drought exposure expressed as the number of months within each decade that a grid cell experienced drought conditions ( $SMI \leq 0.2$ ). The inset histograms show the frequency distribution of cumulative time under drought for all grid cells. The red dashed line indicates the mean duration. E-OBS data is missing for the region shaded grey.

460 2001–2010 experienced virtually no exceptional drought. In cumulative terms, more than half  
 461 of all exceptional drought months in the five-decade record occurred between 2011 and 2020.

### 462 **3.3 Divergence between soil moisture and SPEI droughts**

463 To examine how precipitation-based drought indicators reflect land-surface moisture stress, we  
 464 compared SMI and SPEI patterns during the three most severe soil moisture drought events  
 465 ranked by total drought months (TDM): 1975–1977, 2016–2017, and 2018–2019. Because  
 466 SMI is computed on a monthly timescale, we derived the climatic water balance (precipitation  
 467 minus potential evapotranspiration) from E-OBS and calculated SPEI at one- and three-month  
 468 accumulation periods. Pixel-wise SPEI-1 and SPEI-3 were computed using the SPEI pack-  
 469 age developed by Vonk (2024). We limited the accumulation period to three months because  
 470 this timescale is currently used in operational drought monitoring in Belgium. Since SPEI is

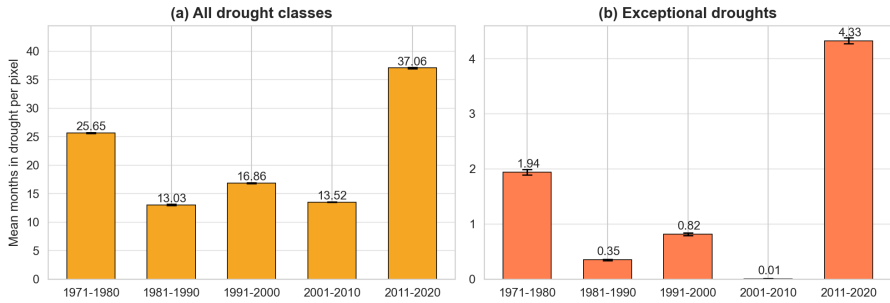


**Fig. 7:** Decadal pixel-wise cumulative drought exposure. The bars show the mean number of months each grid cell spent in drought per decade (not necessarily consecutive), with 95% bootstrap confidence intervals (black whiskers) for (a) All drought classes ( $SMI \leq 0.20$ ) and, (b) exceptional drought only ( $SMI \leq 0.02$ ).

471 anomaly-based rather than percentile-based, we associated  $SPEI = -1.0$  with  $SMI = 0.2$  to  
 472 represent the threshold for at least moderate drought, following the drought severity guide-  
 473 lines of Svoboda et al. (2002). We evaluated the differences between indices in terms of (i)  
 474 anomaly magnitude, (ii) drought persistence (maximum number of *consecutive* months under  
 475 at least moderate drought within an event), and (iii) cumulative drought exposure (total num-  
 476 ber of months, not necessarily consecutive, under at least moderate drought within the event  
 477 window).

478 In terms of anomaly magnitude, SMI generally indicated stronger and longer-lasting  
 479 deficits than SPEI-1 and, to a lesser extent, SPEI-3 (Figure 8). SPEI-1 responds strongly to  
 480 short-lived precipitation anomalies that may not immediately translate into changes in root-  
 481 zone storage. By design, SPEI-3 smooths some of the short-term variability in SPEI-1 and  
 482 more closely resembles the temporal evolution of soil-moisture anomalies, but still tends  
 483 to underestimate deficit magnitude relative to SMI over our domain (Figure 8). Among the  
 484 three events, SMI indicated the strongest soil moisture deficits during 2016–2017 (with SMI  
 485 approaching zero), which is not reflected in either SPEI-1 or SPEI-3. Although the 2016–2017  
 486 drought was interrupted by intermediate wet conditions during March and April 2017, leading  
 487 to partial recovery, this wet spell did not split the event because the month-to-month overlap  
 488 in drought area remained above the  $640 \text{ km}^2$  merging threshold, and the drought therefore  
 489 remained a single multi-temporal event.

490 We also found that SMI-based droughts exhibited higher persistence than SPEI-based  
 491 droughts. Median persistence for SMI was 9 months in 1975–1977, 6 months in 2016–2017,  
 492 and 7 months in 2018–2019 (Table 3). In comparison, SPEI-1 shows much shorter median

493 persistence (3 months in 1975–1977 and 2 months in both 2016–2017 and 2018–2019), while  
 494 SPEI-3 is closer to SMI but remains lower (7 months in 1975–1977 and 5 months in both  
 495 2016–2017 and 2018–2019).

496 The same pattern is evident for cumulative drought exposure. Median cumulative exposure  
 497 for SMI was 10 months in 1975–1977 and 2016–2017 and 8 months in 2018–2019, compared  
 498 with 4, 6, and 3 months for SPEI-1 and 7, 8, and 6 months for SPEI-3 (Table 3, additional  
 499 maps in Supplementary Text S3, Figures S3 and S4).

500 This systematically longer persistence and exposure shown by the SMI indicates that soil  
 501 moisture droughts last longer than precipitation-based droughts because transient precipita-  
 502 tion events do not necessarily translate into root-zone recovery. Additional description on the  
 503 patterns of SMI and SPEI recovery is presented in Supplementary Text S3.

504 The differences presented herein do not imply that one indicator is necessarily *better*;  
 505 rather, they are all useful for demonstrating how a drought shock progressively propagates  
 506 through different components of the hydrological system. Precipitation-based indices like  
 507 SPEI reflect short-term meteorological inputs that may still be agriculturally meaningful. As  
 508 Figure 8 shows, rainfall events during dry periods may not replenish deeper soil moisture due  
 509 to immediate losses through evapotranspiration, yet these events can still temporarily allevi-  
 510 ate plant water stress, especially for fast-responding, shallow-rooted crops or annual crops.  
 511 The recovery of SPEI out of drought conditions may thus signal ‘relief’ that is real, albeit  
 512 short-lived and limited in scope. On the other hand, SMI-based drought analysis better cap-  
 513 tures the persistence of land surface water deficits and the residual moisture stresses that  
 514 continue to affect the dependent ecosystems (e.g., perennial deep-rooted vegetation) long after  
 515 meteorological conditions have normalized.

**Table 3:** Quantified drought persistence and cumulative drought exposure during the three major events (1975–1977, 2016–2017, and 2018–2019) for SMI, SPEI-1, and SPEI-3. Values represent the median across all grid cells in the domain. For cumulative exposure, we additionally report the spatial maximum (in brackets), which represents the time until the last grid cells recover above the moderate-drought threshold within the event window.

Index	Max. consecutive months (persistence)			Total drought months (cumulative exposure)		
	1975–1977	2016–2017	2018–2019	1975–1977	2016–2017	2018–2019
SMI	9	6	7	10 (16)	10 (15)	8 (10)
SPEI-1	3	2	2	4 (7)	6 (8)	3 (5)
SPEI-3	7	5	5	7 (13)	8 (12)	6 (9)

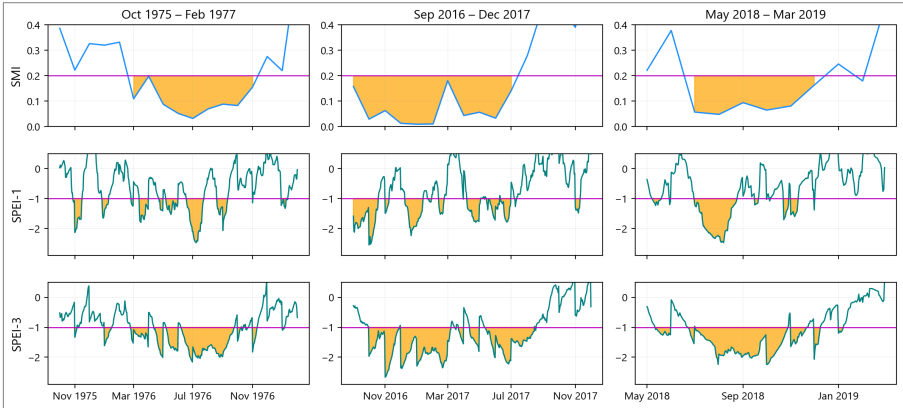


**Fig. 8:** Comparison of domain-average SMI, SPEI-1, and SPEI-3 time series during the three biggest drought events up to 2020. The orange shaded areas indicate drought conditions, defined as  $SMI \leq 0.2$  and  $SPEI \leq -1.0$ . The horizontal magenta lines mark the drought threshold for each index.

## 516 4 Discussion

517 This extended temporal analysis of soil moisture droughts over Belgium offers new insights  
 518 on the severity of recent droughts in the country. Without such a long-term, multi-decadal  
 519 viewpoint, the recent intensification of drought severity and frequency might be mistakenly  
 520 viewed as isolated, transient events rather than as indicators of a potential shift in the climate  
 521 regime. These changes, despite the absence of significant linear trends, also raise important  
 522 questions regarding potential non-linear transitions in regional hydro-climatic equilibria, to  
 523 which we find answers by studying longer reconstructions of the European drought patterns  
 524 from other studies.

525 Our findings are consistent with the wider pan-European narrative of intensifying droughts  
 526 over the continent in the 21<sup>st</sup> century. García-Herrera et al. (2019) showed that drought con-  
 527 ditions covered 90% of central-western Europe from July 2016 to June 2017, with 25% of  
 528 the area in record-breaking severity. This drought led to widespread impacts of agriculture,  
 529 water supplies and hydropower production and was the most severe drought Europe had faced  
 530 between 1979 and 2017. Longer historical reconstructions of European droughts by Hari  
 531 et al. (2020) and Rakovec et al. (2022) show that the occurrence of the consecutive European  
 532 summer droughts of 2018–2019, where 50% of Central Europe was under extreme drought  
 533 conditions, is unprecedented in the last 250 years (since at least 1766). In their synthesis of  
 534 the effect of this drought on crop yields, the same study found that the drought reduced maize  
 535 yields in western Europe by 20-40% and caused about a 10% loss in barley yields for a majority

536 of European countries. By dating stable tree-ring isotopes to reconstruct the summer hydrocli-  
537 mate of central Europe from 75 BCE to 2018 CE, Büntgen et al. (2021) found that the recent  
538 succession of extreme European summer droughts between 2015 and 2018 are unprecedented  
539 in the previous 2,110 years.

540 Various studies attribute atmospheric circulation patterns and the potential role of anthro-  
541 pogenic warming as the dominant drivers of these drought dynamics. Ionita et al. (2020) link  
542 the sustained period of spring droughts in Europe between 2007 and 2020 to a prevalence of  
543 anticyclonic and a persistent blocking high over the North Sea. These conditions deflect west-  
544 erly storms and increase temperature due to a lengthened sunshine duration. This consequently  
545 increases evapotranspiration, which has been found to amplify European summer droughts  
546 (Teuling et al., 2013). García-Herrera et al. (2019) observed that high-latitude atmospheric  
547 blocking contributed to the drought conditions over northwestern Europe in 2016–2017 by  
548 decreasing moisture transport from the Atlantic Ocean. Hari et al. (2020) similarly attributed  
549 the intensification of the 2018–2019 drought to anticyclonic circulation which caused a block-  
550 ing that increased temperature anomalies to +2.8 K in central to northern Europe (Rakovec  
551 et al., 2022). These patterns are projected to persist in the future as anthropogenic warming  
552 weakens the temperature gradient between the polar and mid-latitudinal regions and fluctu-  
553 ates the strength of the jet stream and the persistence of extreme weather events (Cohen et al.,  
554 2014; Dai et al., 2019; Ionita et al., 2020). Europe-wide studies show that anthropogenic warm-  
555 ing will worsen droughts and events of the nature of severity as the 2018–2019 drought will  
556 become routine, persist longer and affect a larger proportion of area (Samaniego et al., 2018;  
557 Hari et al., 2020; Rakovec et al., 2022). These emphasize the need to continue strengthening  
558 drought monitoring and investing in drought preparedness and mitigation measures.

559 On the comparison between precipitation and soil-based drought indicators, we stress that  
560 these indicators are useful for different components of the hydrological system. SPEI-1 and  
561 SPEI-3 may suit analyzing drought patterns in shallow soil layers and shorter temporal scales  
562 but are limited for indicating drought persistence deeper in the soil or in complex ecosystems  
563 due to their ignorance of land-ecosystem interactions (Xu et al., 2021; Peng et al., 2024). When  
564 assessing drought impacts on ecosystems, groundwater recharge, or perennial vegetation like  
565 forests, the divergence between meteorological and soil moisture signals can become com-  
566 plex. In such systems, soil properties such as hydrophobicity during prolonged dry periods can  
567 lead to highly uneven infiltration (Gimbel et al., 2016; Filipović et al., 2018). Heavy summer  
568 rainfall may not be absorbed uniformly across the soil profile but instead run off or infiltrate  
569 preferentially along cracks, roots, or macropores, sometimes bypassing the upper root zone.  
570 While this limits the ability of standard soil moisture indices to reflect actual water availability  
571 near the surface, it may still benefit deep-rooted vegetation like trees by replenishing deeper

572 soil layers (Zhu et al., 2015; Duniway et al., 2018). Assessing drought stress and recovery in  
573 these systems thus requires models and indicators that account for vertical and spatial hetero-  
574 geneity in infiltration and root water uptake (e.g., Shen et al. (2025)), rather than relying solely  
575 on averaged or surface-weighted soil moisture metrics. Further, while it may be argued that  
576 SPEI at longer accumulation periods (e.g., 6, 9 or 12 months) can lead to a closer resemblance  
577 of root-zone moisture conditions, finding the appropriate accumulation lengths is dependent on  
578 landscape and soil characteristics (topography, rooting depth, soil hydrology and management  
579 conditions) and climatic conditions, which can lead to a strong variation of drought characteris-  
580 tics if the landscape is heterogeneous. Kumar et al. (2016) indeed found that applying spatially  
581 variable accumulation periods achieves a higher correlation between precipitation-based and  
582 groundwater drought indices over a uniform domain-wide accumulation period, even at long  
583 accumulation times.

584 Our findings are relevant beyond Belgium because the workflow used in this study can be  
585 transferred to other regions provided that the meteorological forcing is available at appropri-  
586 ate resolution, a hydrological or land-surface model is parameterized to represent soil-water  
587 storage, and consistent long-term simulations can be produced. Extending the analysis to other  
588 domains would allow the same drought dynamics addressed in this study to be evaluated under  
589 different climate gradients, soil, land-cover conditions, and management regimes.

590 From an operational perspective, the results support a monitoring strategy that comple-  
591 ments precipitation-based indices with soil-moisture-based indicators rather than interchang-  
592 ing them. As we have shown, precipitation-based indices are useful for tracking meteorological  
593 anomalies and can provide early signals of emerging drought risk, but they may not capture  
594 persistent impacts when land-surface memory sustains root-zone deficits after rainfall resumes.  
595 In an operational system, precipitation-based indices can be used for early warning, while a  
596 root-zone soil moisture drought indicator is better utilized to track agricultural drought devel-  
597 opment and recovery and to assess when conditions have returned to normal in the soil profile.  
598 These outputs can be integrated into management decisions by linking drought phase and per-  
599 sistence to sector-relevant decisions. For example, soil-moisture drought persistence is directly  
600 relevant for agricultural advisories that inform planting and irrigation planning and signaling  
601 crop yield risk and the risks associated with the occurrence of wildfires or floods that can occur  
602 due to seasonally saturated soils. Slow recovery in soil and catchment storage after meteo-  
603 rological drought can also inform water supply preparedness and groundwater management,  
604 since water resources often show a delayed return to normal conditions (Yang et al., 2017).  
605 For inland navigation and low-flow management, combining soil moisture drought informa-  
606 tion with streamflow indicators can help distinguish short, transient precipitation deficits from  
607 longer-lasting, storage-driven drought conditions. In practice, monthly updates of a root-zone

608 soil moisture drought map, paired with precipitation-based indices, would support earlier iden-  
609 tification of drought evolution and lead to more realistic expectations for recovery following  
610 intermittent wet periods (Van Loon et al., 2024).

## 611 **5 Limitations and future work.**

612 Our results rely on the evaluation of model-derived soil moisture conditions, which are  
613 inevitably constrained by structural, parametric, and forcing uncertainties that we did not  
614 explicitly evaluate. Choices of the mapping between drought categories (e.g.,  $\text{SPEI} = -1.0$  vs.  
615  $\text{SMI} \leq 0.2$ ) and a uniform accumulation period over the whole domain (for SPEI analysis)  
616 also introduce additional subjectivity. The mHM model also does not account for anthro-  
617 pogenic factors such as irrigation, groundwater abstraction, tile drainage and artificial canals,  
618 and land management conditions, which affect the hydrology of the domain. Future work  
619 can partially offset these limitations by quantifying uncertainty using ensembles of forcings,  
620 investigating model parameters to derive confidence intervals for drought magnitude, area, and  
621 timing, incorporating human water use and irrigation processes, or assimilating independent  
622 observations (such as in situ or remotely sensed soil moisture and terrestrial water storage) to  
623 better constrain states and evaluate the joint behaviour of multiple drought indicators alongside  
624 observed impacts.

## 625 **6 Conclusion**

626 This study provides a multi-decadal (1971–2020), high-resolution reconstruction of root-zone  
627 soil moisture droughts over Belgium. Using event-based severity metrics that quantify drought  
628 duration, spatial extent, and intensity, we show that droughts in 2011–2020 occurred about  
629 1.5 times as frequently as during the preceding decades (1971–2010). The 2011–2020 decade  
630 also exhibits the highest share of exceptional drought, exceeding the cumulative occurrence of  
631 exceptional drought across all earlier decades in the record.

632 By comparing soil-moisture drought (SMI) with precipitation-based indicators (SPEI-1  
633 and SPEI-3) for the three most severe events, we show that precipitation-based indices sys-  
634 tematically underestimate drought persistence and cumulative exposure relative to root-zone  
635 soil moisture. In particular, soil moisture droughts persist longer and recover more slowly than  
636 meteorological anomalies, reflecting land-surface memory. Including soil moisture monitoring  
637 in drought observatories thus offers the added value of capturing lingering stresses on agricul-  
638 ture and ecosystems, which can persist long after meteorological conditions have normalized.  
639 This provides decision-makers with a more complete view of drought severity and duration  
640 and supports targeted response and mitigation efforts.

641 The reconstructed drought record and event-based metrics presented in this study pro-  
642 vide a consistent basis for benchmarking recent droughts against historical variability and for  
643 supporting drought monitoring and management.

644 **Author Contributions:**

645 KL, RK and OR formulated the study and set up the model simulations. KL analyzed the  
646 data and prepared the figures with contributions from OR, RK and SD. All authors contributed  
647 to writing and reviewing the contents of the manuscript. All authors read and approved the  
648 contents of the final manuscript.

649 **Acknowledgements:**

650 We acknowledge the work of Jens Wilhelmi (BFG\_Nw network) for providing data in  
651 support of the International Soil Moisture Network. We also acknowledge the work of Arnaud  
652 Blanchouin and ORACLE team of the Institut national de recherche en sciences et technologies  
653 pour l'environnement et l'agriculture, France in support of the ISMN. We are grateful to the High  
654 Performance Computing system of Vrije Universiteit Brussel for providing the computational  
655 resources required to run the model and the analysis of model outputs. We also acknowledge  
656 all the sources of data used in this study for providing the data openly.

657 **Funding:**

658 The authors acknowledge the financial support of the Research Foundation – Flanders  
659 (FWO) for funding the International Coordination Action (ICA) “Open Water Network:  
660 Impacts of Global Change on Water Quality” (project code G0ADS24N). OR acknowl-  
661 edges the Research Excellence in Environmental Sciences (REES) project of the Faculty of  
662 Environmental Sciences, Czech University of Life Sciences Prague.

663 **Data Availability:**

664 All datasets used in this paper are openly available as described in the methodology text.

665 **Code Availability:**

666 The scripts used to arrive at the findings of this study are available at:

667 [https://github.com/klekarkar/pre\\_post\\_process\\_mHM](https://github.com/klekarkar/pre_post_process_mHM).

668 The SMI analysis was carried out using the SMI package, available at:

669 <https://github.com/mhm-ufz/SMI>.

670 **Competing interests:**

671 At least one of the (co-)authors is a member of the editorial board of Hydrology and Earth  
672 System Sciences.

## References

- 673
- 674 Banjara, P., P.K. Shrestha, V.P. Pandey, M. Sah, and P. Panday. 2025, February. Quantifying  
675 agricultural drought in the Koshi River basin through soil moisture simulation. *Journal of*  
676 *Hydrology: Regional Studies* 57: 102132. <https://doi.org/10.1016/j.ejrh.2024.102132> .
- 677 Bastos, A., P. Ciaais, P. Friedlingstein, S. Sitch, J. Pongratz, L. Fan, J.P. Wigneron, U. Weber,  
678 M. Reichstein, Z. Fu, P. Anthoni, A. Arneth, V. Haverd, A.K. Jain, E. Joetzjer, J. Knauer,  
679 S. Lienert, T. Loughran, P.C. McGuire, H. Tian, N. Viovy, and S. Zaehle. 2020, June. Direct  
680 and seasonal legacy effects of the 2018 heat wave and drought on European ecosystem  
681 productivity. *Science Advances* 6(24): eaba2724. <https://doi.org/10.1126/sciadv.aba2724> .
- 682 Beck, H.E., T.R. McVicar, N. Vergopolan, A. Berg, N.J. Lutsko, A. Dufour, Z. Zeng, X. Jiang,  
683 A.I.J.M. Van Dijk, and D.G. Miralles. 2023, October. High-resolution (1 km) Köppen-  
684 Geiger maps for 1901–2099 based on constrained CMIP6 projections. *Scientific Data* 10(1):  
685 724. <https://doi.org/10.1038/s41597-023-02549-6> .
- 686 Beckers, V., J. Beckers, M. Vanmaercke, E. Van Hecke, A. Van Rompaey, and N. Dendoncker.  
687 2018, September. Modelling Farm Growth and Its Impact on Agricultural Land Use: A  
688 Country Scale Application of an Agent-Based Model. *Land* 7(3): 109. <https://doi.org/10.3390/land7030109> .
- 690 Beckers, V., L. Poelmans, A. Van Rompaey, and N. Dendoncker. 2020, September. The impact  
691 of urbanization on agricultural dynamics: a case study in Belgium. *Journal of Land Use*  
692 *Science* 15(5): 626–643. <https://doi.org/10.1080/1747423X.2020.1769211> .
- 693 Boeing, F., O. Rakovec, R. Kumar, L. Samaniego, M. Schrön, A. Hildebrandt, C. Rebmann,  
694 S. Thober, S. Müller, S. Zacharias, H. Bogena, K. Schneider, R. Kiese, S. Attinger, and  
695 A. Marx. 2022, October. High-resolution drought simulations and comparison to soil mois-  
696 ture observations in Germany. *Hydrology and Earth System Sciences* 26(19): 5137–5161.  
697 <https://doi.org/10.5194/hess-26-5137-2022> .
- 698 Bogena, H., C. Montzka, J. Huisman, A. Graf, M. Schmidt, M. Stockinger, C. Von Hebel,  
699 H. Hendricks-Franssen, J. Van Der Kruk, W. Tappe, A. Lücke, R. Baatz, R. Bol, J. Groh,  
700 T. Pütz, J. Jakobi, R. Kunkel, J. Sorg, and H. Vereecken. 2018, January. The TERENO-  
701 Rur Hydrological Observatory: A Multiscale Multi-Compartment Research Platform for the  
702 Advancement of Hydrological Science. *Vadose Zone Journal* 17(1): 1–22. <https://doi.org/10.2136/vzj2018.03.0055> .  
703

704 Bonan, G.B. and L.M. Stillwell-Soller. 1998. Soil water and the persistence of floods and  
705 droughts in the Mississippi River Basin. *Water Resources Research* 34(10): 2693–2701 .

706 Brisson, E., M. Demuzere, B. Kwakernaak, and N.P.M. Van Lipzig. 2011, February. Rela-  
707 tions between atmospheric circulation and precipitation in Belgium. *Meteorology and*  
708 *Atmospheric Physics* 111(1): 27–39. <https://doi.org/10.1007/s00703-010-0103-y> .

709 Büntgen, U., O. Urban, P.J. Krusic, M. Rybníček, T. Kolář, T. Kyncl, A. Ač, E. Koňasová,  
710 J. Čáslavský, J. Esper, S. Wagner, M. Saurer, W. Tegel, P. Dobrovolný, P. Cherubini,  
711 F. Reinig, and M. Trnka. 2021, April. Recent European drought extremes beyond Common  
712 Era background variability. *Nature Geoscience* 14(4): 190–196. <https://doi.org/10.1038/s41561-021-00698-0> .

714 Cao, S., M. Li, Z. Zhu, Z. Wang, J. Zha, W. Zhao, Z. Duanmu, J. Chen, Y. Zheng, Y. Chen,  
715 et al. 2023. Spatiotemporally consistent global dataset of the gimms leaf area index (gimms  
716 lai4g) from 1982 to 2020. *Earth System Science Data* 15(11): 4877–4899 .

717 Chini, M. 2022, July. Code red: Temperatures up to 40°C in belgium today. [https://www.](https://www.brusselstimes.com/belgium/258298/code-red-temperatures-up-to-40c-in-belgium-today)  
718 [brusselstimes.com/belgium/258298/code-red-temperatures-up-to-40c-in-belgium-today](https://www.brusselstimes.com/belgium/258298/code-red-temperatures-up-to-40c-in-belgium-today).  
719 The Brussels Times, accessed April 8, 2025.

720 Cohen, J., J.A. Screen, J.C. Furtado, M. Barlow, D. Whittleston, D. Coumou, J. Francis,  
721 K. Dethloff, D. Entekhabi, J. Overland, et al. 2014. Recent arctic amplification and extreme  
722 mid-latitude weather. *Nature geoscience* 7(9): 627–637 .

723 Copernicus Climate Change Service. 2022. European State of the Climate - Summary  
724 2022. <https://climate.copernicus.eu/esotc/2022/european-state-climate-2022-summary>.  
725 Accessed: 2025-04-08.

726 Cornes, R.C., G. Van Der Schrier, E.J. Van Den Besselaar, and P.D. Jones. 2018. An ensemble  
727 version of the e-obs temperature and precipitation data sets. *Journal of Geophysical*  
728 *Research: Atmospheres* 123(17): 9391–9409 .

729 Dai, A., D. Luo, M. Song, and J. Liu. 2019. Arctic amplification is caused by sea-ice loss  
730 under increasing co2. *Nature communications* 10(1): 121 .

731 De Ridder, K., K. Coudere, M. Depoorter, I. Liekens, X. Pourria, D. Steinmetz, E. Vanuytrecht,  
732 K. Verhaegen, and H. Wouters 2020, July. Evaluation of the socio-economic impact of  
733 climate change in belgium. Summary for policymakers, National Climate Commission.  
734 Study commissioned by the National Climate Commission.

- 735 Dembélé, M., M. Hrachowitz, H.H.G. Savenije, G. Mariétoz, and B. Schaefli. 2020, Jan-  
736 uary. Improving the Predictive Skill of a Distributed Hydrological Model by Calibration  
737 on Spatial Patterns With Multiple Satellite Data Sets. *Water Resources Research* 56(1):  
738 e2019WR026085. <https://doi.org/10.1029/2019WR026085> .
- 739 Demirel, M., J. Koch, O. Rakovec, R. Kumar, J. Mai, S. Müller, S. Thober, L. Samaniego, and  
740 S. Stisen. 2024. Tradeoffs between temporal and spatial pattern calibration and their impacts  
741 on robustness and transferability of hydrologic model parameters to ungauged basins. *Water*  
742 *Resources Research* 60(1). <https://doi.org/https://doi.org/10.1029/2022WR034193> .
- 743 Dirmeyer, P.A., Z. Guo, and X. Gao. 2004. Comparison, validation, and transferability of eight  
744 multiyear global soil wetness products. *Journal of Hydrometeorology* 5(6): 1011–1033 .
- 745 Dorigo, W., I. Himmelbauer, D. Aberer, L. Schremmer, I. Petrakovic, L. Zappa, W. Preimes-  
746 berger, A. Xaver, F. Annor, J. Ardö, et al. 2021. The international soil moisture network:  
747 serving earth system science for over a decade. *Hydrology and Earth System Sciences*  
748 *Discussions* 2021: 1–83 .
- 749 Dorigo, W., A. Xaver, M. Vreugdenhil, A. Gruber, A. Hegyiova, A.D. Sanchis-Dufau,  
750 D. Zamojski, C. Cordes, W. Wagner, and M. Drusch. 2013. Global automated quality con-  
751 trol of in situ soil moisture data from the international soil moisture network. *Vadose Zone*  
752 *Journal* 12(3): vjz2012–0097 .
- 753 DOV. 2025. Databank Ondergrond Vlaanderen: Actuele grondwaterstandindicator. [https://](https://www.dov.vlaanderen.be/page/actuele-grondwaterstandindicator)  
754 [www.dov.vlaanderen.be/page/actuele-grondwaterstandindicator](https://www.dov.vlaanderen.be/page/actuele-grondwaterstandindicator). Accessed 27 Oct 2025.
- 755 Duniway, M.C., M.D. Petrie, D.P.C. Peters, J.P. Anderson, K. Crossland, and J.E. Herrick.  
756 2018, July. Soil water dynamics at 15 locations distributed across a desert landscape:  
757 insights from a 27-yr dataset. *Ecosphere* 9(7): e02335. <https://doi.org/10.1002/ecs2.2335> .
- 758 Erpicum, M., M. Nouri, and A. Demoulin. 2018. The Climate of Belgium and Luxembourg, In  
759 *Landscapes and Landforms of Belgium and Luxembourg*, ed. Demoulin, A., 35–41. Cham:  
760 Springer International Publishing. [https://doi.org/10.1007/978-3-319-58239-9\\_3](https://doi.org/10.1007/978-3-319-58239-9_3).
- 761 European Commission, Joint Research Centre 2011. Drought news in Europe: Situation in  
762 April 2011. Technical report, European Drought Observatory (EDO). Accessed: 2025-09-  
763 01.
- 764 European Environment Agency. 2023, October. Drought impact on  
765 ecosystems in europe. <https://www.eea.europa.eu/en/analysis/indicators/>

drought-impact-on-ecosystems-in-europe. Accessed: 2025-04-08.

Farr, T.G., P.A. Rosen, E. Caro, R. Crippen, R. Duren, S. Hensley, M. Kobrick, M. Paller, E. Rodriguez, L. Roth, et al. 2007. The shuttle radar topography mission. *Reviews of geophysics* 45(2) .

Feddes, R.A. 1982. Simulation of field water use and crop yield, *Simulation of plant growth and crop production*, 194–209. Pudoc.

Filipović, V., T. Weninger, L. Filipović, A. Schwen, K.L. Bristow, S. Zechmeister-Boltenstern, and S. Leitner. 2018, June. Inverse estimation of soil hydraulic properties and water repellency following artificially induced drought stress. *Journal of Hydrology and Hydromechanics* 66(2): 170–180. <https://doi.org/10.2478/johh-2018-0002> .

Ford, T.W. and S.M. Quiring. 2019, February. Comparison of Contemporary In Situ, Model, and Satellite Remote Sensing Soil Moisture With a Focus on Drought Monitoring. *Water Resources Research* 55(2): 1565–1582. <https://doi.org/10.1029/2018WR024039> .

García-Herrera, R., J.M. Garrido-Perez, D. Barriopedro, C. Ordóñez, S.M. Vicente-Serrano, R. Nieto, L. Gimeno, R. Sorí, and P. Yiou. 2019, June. The European 2016/17 Drought. *Journal of Climate* 32(11): 3169–3187. <https://doi.org/10.1175/JCLI-D-18-0331.1> .

Gimbel, K.F., H. Puhlmann, and M. Weiler. 2016, April. Does drought alter hydrological functions in forest soils? *Hydrology and Earth System Sciences* 20(3): 1301–1317. <https://doi.org/10.5194/hess-20-1301-2016> .

Goudenhoofdt, E. and L. Delobbe. 2013, April. Statistical Characteristics of Convective Storms in Belgium Derived from Volumetric Weather Radar Observations. *Journal of Applied Meteorology and Climatology* 52(4): 918–934. <https://doi.org/10.1175/JAMC-D-12-079.1> .

Hargreaves, G.H. and Z.A. Samani. 1985. Reference crop evapotranspiration from temperature. *Applied engineering in agriculture* 1(2): 96–99 .

Hari, V., O. Rakovec, Y. Markonis, M. Hanel, and R. Kumar. 2020, August. Increased future occurrences of the exceptional 2018–2019 Central European drought under global warming. *Scientific Reports* 10(1): 12207. <https://doi.org/10.1038/s41598-020-68872-9> .

Hartmann, J. and N. Moosdorf. 2012. The new global lithological map database glim: A representation of rock properties at the earth surface. *Geochemistry, Geophysics*,

796 *Geosystems* 13(12) .

797 Ionita, M., V. Nagavciuc, R. Kumar, and O. Rakovec. 2020, December. On the curious case  
798 of the recent decade, mid-spring precipitation deficit in central Europe. *npj Climate and*  
799 *Atmospheric Science* 3(1): 49. <https://doi.org/10.1038/s41612-020-00153-8> .

800 Jarvis, N. 1989. A simple empirical model of root water uptake. *Journal of Hydrology* 107(1-  
801 4): 57–72 .

802 Journée, M., C. Delvaux, and C. Bertrand. 2015, April. Precipitation climate maps of Belgium.  
803 *Advances in Science and Research* 12(1): 73–78. <https://doi.org/10.5194/asr-12-73-2015> .

804 Koster, R.D., Z. Guo, R. Yang, P.A. Dirmeyer, K. Mitchell, and M.J. Puma. 2009. On the  
805 nature of soil moisture in land surface models. *Journal of Climate* 22(16): 4322–4335 .

806 Kumar, R., J.L. Musuuza, A.F. Van Loon, A.J. Teuling, R. Barthel, J. Ten Broek, J. Mai,  
807 L. Samaniego, and S. Attinger. 2016, March. Multiscale evaluation of the Standardized  
808 Precipitation Index as a groundwater drought indicator. *Hydrology and Earth System*  
809 *Sciences* 20(3): 1117–1131. <https://doi.org/10.5194/hess-20-1117-2016> .

810 Kumar, R., L. Samaniego, and S. Attinger. 2013. Implications of distributed hydrologic  
811 model parameterization on water fluxes at multiple scales and locations. *Water Resources*  
812 *Research* 49(1): 360–379 .

813 Kumar, R., L. Samaniego, S. Thober, O. Rakovec, A. Marx, N. Wanders, M. Pan, F. Hesse,  
814 and S. Attinger. 2025, January. Multi-Model Assessment of Groundwater Recharge Across  
815 Europe Under Warming Climate. *Earth's Future* 13(1): e2024EF005020. [https://doi.org/](https://doi.org/10.1029/2024EF005020)  
816 [10.1029/2024EF005020](https://doi.org/10.1029/2024EF005020) .

817 Livneh, B., R. Kumar, and L. Samaniego. 2015. Influence of soil textural properties on hydro-  
818 logic fluxes in the mississippi river basin. *Hydrological Processes* 29(21): 4638–4655  
819 .

820 Meersmans, J., K. Van Weverberg, S. De Baets, F. De Ridder, S. Palmer, B. Van Wesemael, and  
821 T. Quine. 2016, September. Mapping mean total annual precipitation in Belgium, by inves-  
822 tigating the scale of topographic control at the regional scale. *Journal of Hydrology* 540:  
823 96–105. <https://doi.org/10.1016/j.jhydrol.2016.06.013> .

824 Mishra, A.K. and V.P. Singh. 2010. A review of drought concepts. *Journal of hydrology* 391(1-  
825 2): 202–216 .

826 Moravec, V., Y. Markonis, O. Rakovec, R. Kumar, and M. Hanel. 2019, June. A 250-Year  
827 European Drought Inventory Derived From Ensemble Hydrologic Modeling. *Geophysical*  
828 *Research Letters* 46(11): 5909–5917. <https://doi.org/10.1029/2019GL082783> .

829 Nachtergaele, F., H. van Velthuizen, L. Verelst, D. Wiberg, M. Henry, F. Chiozza, Y. Yigini,  
830 E. Aksoy, N. Batjes, E. Boateng, et al. 2023. *Harmonized world soil database version 2.0*.  
831 FAO.

832 Nicholson, S. 2000. Land surface processes and Sahel climate. *Reviews of Geophysics* 38(1):  
833 117–139 .

834 Nicolai-Shaw, N., M. Hirschi, H. Mittelbach, and S.I. Seneviratne. 2015, October. Spatial  
835 representativeness of soil moisture using in situ, remote sensing, and land reanalysis data.  
836 *Journal of Geophysical Research: Atmospheres* 120(19): 9955–9964. [https://doi.org/10.](https://doi.org/10.1002/2015JD023305)  
837 [1002/2015JD023305](https://doi.org/10.1002/2015JD023305) .

838 Peng, C., J. Zeng, K.S. Chen, H. Ma, H. Letu, X. Zhang, P. Shi, and H. Bi. 2025. Spatial  
839 Representativeness of Soil Moisture Stations and Its Influential Factors at a Global Scale.  
840 *IEEE Transactions on Geoscience and Remote Sensing* 63: 1–15. [https://doi.org/10.1109/](https://doi.org/10.1109/TGRS.2024.3523484)  
841 [TGRS.2024.3523484](https://doi.org/10.1109/TGRS.2024.3523484) .

842 Peng, L., J. Sheffield, Z. Wei, M. Ek, and E.F. Wood. 2024, September. An enhanced  
843 Standardized Precipitation–Evapotranspiration Index (SPEI) drought-monitoring method  
844 integrating land surface characteristics. *Earth System Dynamics* 15(5): 1277–1300. [https:](https://doi.org/10.5194/esd-15-1277-2024)  
845 [//doi.org/10.5194/esd-15-1277-2024](https://doi.org/10.5194/esd-15-1277-2024) .

846 Rakovec, O., N. Mizukami, R. Kumar, A.J. Newman, S. Thober, A.W. Wood, M.P. Clark,  
847 and L. Samaniego. 2019, December. Diagnostic Evaluation of Large-Domain Hydrologic  
848 Models Calibrated Across the Contiguous United States. *Journal of Geophysical Research:*  
849 *Atmospheres* 124(24): 13991–14007. <https://doi.org/10.1029/2019JD030767> .

850 Rakovec, O., L. Samaniego, V. Hari, Y. Markonis, V. Moravec, S. Thober, M. Hanel, and  
851 R. Kumar. 2022, March. The 2018–2020 Multi-Year Drought Sets a New Benchmark in  
852 Europe. *Earth's Future* 10(3): e2021EF002394. <https://doi.org/10.1029/2021EF002394> .

853 Řehoř, J., R. Brázdil, O. Rakovec, M. Hanel, M. Fischer, R. Kumar, J. Balek, M. Poděbradská,  
854 V. Moravec, L. Samaniego, et al. 2025. Global catalog of soil moisture droughts over the  
855 past four decades. *Hydrology and Earth System Sciences* 29(14): 3341–3358 .

856 Royal Forestry Society of Belgium. 2025. Belgium's forests in figures. [https://srfb.be/en/  
857 informations-on-forests/belgium-forests/](https://srfb.be/en/informations-on-forests/belgium-forests/). Last accessed 02 Sep 2025.

858 Samaniego, L., R. Kumar, and S. Attinger. 2010, May. Multiscale parameter regionaliza-  
859 tion of a grid-based hydrologic model at the mesoscale. *Water Resources Research* 46(5):  
860 2008WR007327. <https://doi.org/10.1029/2008WR007327> .

861 Samaniego, L., R. Kumar, and C. Jackisch. 2011. Predictions in a data-sparse region using  
862 a regionalized grid-based hydrologic model driven by remotely sensed data. *Hydrology  
863 Research* 42(5): 338–355 .

864 Samaniego, L., R. Kumar, and M. Zink. 2013, February. Implications of Parameter Uncertainty  
865 on Soil Moisture Drought Analysis in Germany. *Journal of Hydrometeorology* 14(1): 47–68.  
866 <https://doi.org/10.1175/JHM-D-12-075.1> .

867 Samaniego, L., S. Thober, R. Kumar, N. Wanders, O. Rakovec, M. Pan, M. Zink, J. Sheffield,  
868 E.F. Wood, and A. Marx. 2018, May. Anthropogenic warming exacerbates European  
869 soil moisture droughts. *Nature Climate Change* 8(5): 421–426. [https://doi.org/10.1038/  
870 s41558-018-0138-5](https://doi.org/10.1038/s41558-018-0138-5) .

871 Seneviratne, S.I., D. Lüthi, M. Litschi, and C. Schär. 2006. Land–atmosphere coupling and  
872 climate change in europe. *Nature* 443(7108): 205–209 .

873 Sheffield, J., G. Goteti, F. Wen, and E.F. Wood. 2004, December. A simulated soil mois-  
874 ture based drought analysis for the United States. *Journal of Geophysical Research:  
875 Atmospheres* 109(D24): 2004JD005182. <https://doi.org/10.1029/2004JD005182> .

876 Shen, X., J. Liu, X. Han, H. Yang, H. Liu, and F. Ni. 2025, January. Modelling Infiltration  
877 Based on Source-Responsive Method for Improving Simulation of Rapid Subsurface  
878 Stormflow. *Water Resources Research* 61(1): e2024WR037487. [https://doi.org/10.1029/  
879 2024WR037487](https://doi.org/10.1029/2024WR037487) .

880 Shrestha, P., L. Samaniego, O. Rakovec, R. Kumar, and S. Thober. 2025. A novel stream  
881 network upscaling scheme for accurate local streamflow simulations in gridded global  
882 hydrological models. *Water Resources Research* 61(6): e2024WR038183 .

883 Sousa-Silva, R., Q. Ponette, K. Verheyen, A. Van Herzele, and B. Muys. 2016, September.  
884 Adaptation of forest management to climate change as perceived by forest owners and man-  
885 agers in Belgium. *Forest Ecosystems* 3(1): 22. [https://doi.org/10.1186/s40663-016-0082-7  
886 .](https://doi.org/10.1186/s40663-016-0082-7)

887 Statbel. 2025a. Land use. <https://statbel.fgov.be/en/themes/environment/land-cover-and-use/>  
888 land-use. Last accessed 02 Sep 2025.

889 Statbel. 2025b. Population density. [https://statbel.fgov.be/en/news/population-density-385-](https://statbel.fgov.be/en/news/population-density-385-inhabitants-km2-belgium)  
890 inhabitants-km2-belgium.

891 Svoboda, M., D. LeComte, M. Hayes, R. Heim, K. Gleason, J. Angel, B. Rippey, R. Tinker,  
892 M. Palecki, D. Stooksbury, D. Miskus, and S. Stephens. 2002, August. THE DROUGHT  
893 MONITOR. *Bulletin of the American Meteorological Society* 83(8): 1181–1190. <https://doi.org/10.1175/1520-0477-83.8.1181> .

895 Teuling, A.J., A.F. Van Loon, S.I. Seneviratne, I. Lehner, M. Aubinet, B. Heinesch, C. Bern-  
896 hofer, T. Grünwald, H. Prasse, and U. Spank. 2013, May. Evapotranspiration amplifies  
897 European summer drought. *Geophysical Research Letters* 40(10): 2071–2075. <https://doi.org/10.1002/grl.50495> .

899 Tröltzsch, J., R. Vidaurre, H. Bressers, A. Browne, I. La Jeunesse, M. Lordkipanidze,  
900 W. Defloor, W. Maetens, and K. Cauwenberghs. 2016. Flanders: Regional Organiza-  
901 tion of Water and Drought and Using Data as Driver for Change, In *Governance for*  
902 *Drought Resilience*, eds. Bressers, H., N. Bressers, and C. Larrue, 139–158. Cham: Springer  
903 International Publishing. [https://doi.org/10.1007/978-3-319-29671-5\\_7](https://doi.org/10.1007/978-3-319-29671-5_7).

904 Van Loon, A.F., S. Kchouk, A. Matanó, F. Tootoonchi, C. Alvarez-Garreton, K.E. Hassaballah,  
905 M. Wu, M.L. Wens, A. Shyrokaya, E. Ridolfi, et al. 2024. Drought as a continuum–memory  
906 effects in interlinked hydrological, ecological, and social systems. *Natural Hazards and*  
907 *Earth System Sciences* 24(9): 3173–3205 .

908 Vicente-Serrano, S.M., S. Beguería, and J.I. López-Moreno. 2010, April. A Multiscalar  
909 Drought Index Sensitive to Global Warming: The Standardized Precipitation Evapotranspi-  
910 ration Index. *Journal of Climate* 23(7): 1696–1718. <https://doi.org/10.1175/2009JCLI2909>.  
911 1 .

912 VMM. 2023. Toestand van het watersysteem. [https://waterinfo.vlaanderen.be/download/](https://waterinfo.vlaanderen.be/download/c91f13e4-5971-4631-9c35-bf30c3927743?dl=0)  
913 [c91f13e4-5971-4631-9c35-bf30c3927743?dl=0](https://waterinfo.vlaanderen.be/download/c91f13e4-5971-4631-9c35-bf30c3927743?dl=0). Accessed 6 Dec 2025.

914 Vonk, M.A. 2024. SPEI: A simple Python package to calculate and visualize drought indices.

915 Wang, A., D.P. Lettenmaier, and J. Sheffield. 2011a. Soil moisture drought in china, 1950–  
916 2006. *Journal of Climate* 24(13): 3257–3271 .

917 Wang, A., D.P. Lettenmaier, and J. Sheffield. 2011b, July. Soil Moisture Drought in China,  
918 1950–2006. *Journal of Climate* 24(13): 3257–3271. <https://doi.org/10.1175/2011JCLI3733>.  
919 1 .

920 Wu, W., M.A. Geller, and R.E. Dickinson. 2002. The response of soil moisture to long-term  
921 variability of precipitation. *Journal of Hydrometeorology* 3(5): 604–613 .

922 Xaver, A., L. Zappa, G. Rab, I. Pfeil, M. Vreugdenhil, D. Hemment, and W.A. Dorigo. 2020,  
923 April. Evaluating the suitability of the consumer low-cost Parrot Flower Power soil moisture  
924 sensor for scientific environmental applications. *Geoscientific Instrumentation, Methods  
925 and Data Systems* 9(1): 117–139. <https://doi.org/10.5194/gi-9-117-2020> .

926 Xu, Z.g., Z.y. Wu, H. He, X. Guo, and Y.l. Zhang. 2021, September. Comparison of soil mois-  
927 ture at different depths for drought monitoring based on improved soil moisture anomaly  
928 percentage index. *Water Science and Engineering* 14(3): 171–183. [https://doi.org/10.1016/  
929 j.wse.2021.08.008](https://doi.org/10.1016/j.wse.2021.08.008) .

930 Yang, Y., T.R. McVicar, R.J. Donohue, Y. Zhang, M.L. Roderick, F.H. Chiew, L. Zhang, and  
931 J. Zhang. 2017. Lags in hydrologic recovery following an extreme drought: Assessing the  
932 roles of climate and catchment characteristics. *Water Resources Research* 53(6): 4821–4837  
933 .

934 Zhu, L., H. Gong, Z. Dai, T. Xu, and X. Su. 2015, September. An integrated assessment  
935 of the impact of precipitation and groundwater on vegetation growth in arid and semi-  
936 arid areas. *Environmental Earth Sciences* 74(6): 5009–5021. [https://doi.org/10.1007/  
937 s12665-015-4513-5](https://doi.org/10.1007/s12665-015-4513-5) .

938 Zink, M., R. Kumar, M. Cuntz, and L. Samaniego. 2017. A high-resolution dataset of water  
939 fluxes and states for germany accounting for parametric uncertainty. *Hydrology and Earth  
940 System Sciences* 21(3): 1769–1790 .

941 Zreda, M., D. Desilets, T.P.A. Ferré, and R.L. Scott. 2008, November. Measuring soil moisture  
942 content non-invasively at intermediate spatial scale using cosmic-ray neutrons. *Geophysical  
943 Research Letters* 35(21): 2008GL035655. <https://doi.org/10.1029/2008GL035655> .